Leishmania dual-specificity tyrosine-regulated kinase 1 (DYRK1) is required for sustaining Leishmania stationary phase phenotype

Vinícius Pinto Costa Rocha, Mariko Dacher, Simon Alan Young, Foteini Kolokousi, Antonia Efstathiou, Gerald F Späth, Milena Botelho Pereira Soares, Despina Smirlis

Leishmania Dual Specificity Tyrosine Regulated Kinase 1 (DYRK1) is required for sustaining *Leishmania* stationary phase phenotype

Running Title: *Lin*DYRK1 is essential for *Leishmania* stationary phase biology

Vinícius Pinto Costa Rocha[1,2], Mariko Dacher[3#a], Simon Alan Young[4], Foteini Kolokousi[5], Antonia Efstathiou[5], Gerald Frank Späth[3], Milena Botelho Pereira Soares[1,2]*, Despina Smirlis[5]*

[1]Instituto Gonçalo Moniz, Fundação Oswaldo Cruz (FIOCRUZ), Rua Waldemar Falcão 121, Salvador, BA, Brazil;

[2]Centro de Biotecnologia e Terapia Celular, Hospital São Rafael, Avenida São Rafael 2152, Salvador, BA, Brazil;

[3]Unité de Parasitologie Moléculaire et Signalisation, Department of Parasites and Insect Vectors, Institut Pasteur and INSERM U1201, Paris, France;

[4]Biomedical Sciences Research Complex, School of Biology, The University of St. Andrews, North Haugh, St. Andrews, Fife, Scotland, UK;

[5]Molecular Parasitology Laboratory, Microbiology Department, Hellenic Pasteur Institute, 127 Bas. Sofias Avenue, Athens, Greece;

[#a]Current address: Laboratory of Chromatin Structure and Function, Institute for Quantitative Biosciences, The University of Tokyo, Yayoi 1-1-1, Bunkyo-ku, Tokyo, Japan.

Address correspondence to: **1**: Despina Smirlis, Department of Microbiology, Laboratory of Molecular Parasitology, Hellenic Pasteur Institute, 127 Bas. Sofias Avenue, 115 21 Athens, Greece, Tel.: +30 2106478841 Fax: +30 2106423498; e-mail address: penny@pasteur.gr; **2**: Milena Botelho Pereira Soares, Instituto Gonçalo Moniz, Fundação Oswaldo Cruz (FIOCRUZ), Rua Waldemar Falcão 121, Salvador, BA, Brazil; [2]Centro de Biotecnologia e Terapia Celular, Hospital São Rafael, Avenida São Rafael 2152, Salvador, BA, Brazil, Tel: Phone: (+55)71-31762292, email: milena@bahia.fiocruz.br, milenabpsoares@gmail.com

Keywords: *Leishmania*, DYRK, differentiation, cell cycle, growth arrest

Summary

Although the multiplicative and growth-arrested states play key roles in *Leishmania* development, the regulators of these transitions are largely unknown. In an attempt to gain a better understanding of these processes, we characterised one member of a family of protein kinases with dual specificity, *Lin*DYRK1, which acts as a stasis regulator in other organisms. *Lin*DYRK1 over-expressing parasites displayed a decrease in proliferation and in cell cycle re-entry of arrested cells. Parasites lacking *Lin*DYRK1 displayed distinct fitness phenotypes in logarithmic and stationary growth phases. In logarithmic growth-phase, *Lin*DYRK1$^{-/-}$ parasites proliferated better than control lines, supporting a role of this kinase in stasis, while in stationary growth-phase, *Lin*DYRK1$^{-/-}$ parasites had important defects as they rounded up, accumulated vacuoles and lipid bodies and displayed subtle but consistent differences in lipid composition. Moreover, they expressed less metacyclic-enriched transcripts, displayed increased sensitivity to complement lysis and a significant reduction in survival within peritoneal macrophages. The distinct *Lin*DYRK1$^{-/-}$ growth phase phenotypes were mirrored by the distinct *Lin*DYRK1 localisations in logarithmic (flagellar pocket and endosomes) and late stationary phase (mitochondrion). Overall, this work provides first evidence for the role of a DYRK family member in sustaining promastigote stationary phase phenotype and infectivity.

Keywords: *Leishmania***,** DYRK, differentiation, cell cycle, growth arrest

Introduction

Leishmania is a protozoan parasite responsible for a group of diseases, termed leishmaniases, that shows multiple clinical manifestations, ranging from self-healing cutaneous to lethal visceral leishmaniasis if left untreated (Murray *et al.*, 2005). These diseases are endemic in tropical and

subtropical countries, causing severe morbidity and mortality and presenting a worldwide incidence of approximately 1 500 000 clinically reported cases (Alvar *et al.*, 2012).

Leishmania spp have a digenetic life cycle, involving a motile, extracellular promastigote stage that parasitises the alimentary tract of a sand-fly vector, and an immotile amastigote stage that survives and replicates in the phagolysosomes of mononuclear phagocytes (Bates, 1994, Sacks & Perkins, 1984). To complete its life cycle, the parasite has to successfully undergo different developmental transitions induced by environmental stimuli. In the midgut of the sand-fly, sequential development of promastigotes inside the sugar-rich environment initially involves the rapid division of non-infective procyclic promastigotes (Burchmore & Barrett, 2001, McConville & Naderer, 2011). These parasites differentiate into distinct forms, including the cell cycle arrested nectomonads and the dividing leptomonads that will ultimately differentiate to infective, metacyclic promastigotes in the anterior parts of the digestive tract (Gossage *et al.*, 2003). During a blood meal, metacyclics will be transmitted to the mammalian host, where they will encounter a marked environmental temperature (26˚C to 34-37˚C) and pH (7.4 to 5.5) shift, as well as changes in nutrients including a sugar-poor and fatty-acid- and amino-acid-rich environment. Parasites that will successfully adapt to these new environmental changes and subvert the immune system of the host will differentiate and proliferate as amastigotes (Burchmore & Barrett, 2001, McConville & Naderer, 2011).

Leishmania promastigote differentiation in the sand-fly requires homeostatic control and signalling events that are largely unknown (Sacks & Perkins, 1984, Sacks & Perkins, 1985). Procyclic to metacyclic promastigote transitions in the sand fly can be mirrored in cell culture (Gossage *et al.*, 2003) and are characterised by specific molecular, morphological, biochemical and cell cycle changes (Inbar *et al.*, 2017, Sacks *et al.*, 1985, Sacks & Perkins, 1984, Sacks & Perkins, 1985). These transitions are initiated by environmental changes (Cunningham *et al.*, 2001, Serafim *et al.*, 2012), and are communicated by signalling cascades, including phosphosignalling events (Tsigankov *et al.*, 2014, Tsigankov *et al.*, 2013). Despite the importance

of phosphosignalling in differentiation, there is little knowledge on the nature of kinases that mediate these transitions. Amongst these, protein kinase A (PKA) activity is known to be required for the promastigote to amastigote transition (Bachmaier *et al.*, 2016), whereas Target of Rapamycin (TOR) 3 is known to be associated with the development of the infectious stage (Madeira da Silva & Beverley, 2010).

The dual specificity tyrosine regulated kinases (DYRKs) are members of the CMGC group of kinases (Kannan & Neuwald, 2004) are characterised by their dual specificity, presenting an auto-phosphorylation activity of a critical tyrosine residue of the activation loop and a serine/threonine kinase activity towards substrates (Becker & Joost, 1999). Based on the homology of their kinase domain, these proteins are divided into 3 subfamilies: the homeodomain-interacting protein kinases (HIPKs) known to regulate a wide variety of stress signals (Schmitz *et al.*, 2014), the pre-mRNA processing protein 4 kinases (PRP4s) involved in pre-mRNA processing and transcriptional regulation (Huang *et al.*, 2000) and the DYRKs (Aranda *et al.*, 2011). The DYRK subfamily comprises of the YAKs, class I (DYRK1A and DYRK1B) and class II (DYRK2, DYRK3 and DYRK4) DYRKs (Aranda *et al.*, 2011).

The DYRK subfamily members are multifaceted kinases, regulating a great variety of cellular processes including gene expression, proteasomal degradation, or chromatin remodelling. Stasis regulation and differentiation however, is the hallmark of DYRK activity (Aranda *et al.*, 2011). The DYRK subfamily shares a conserved structure which includes a DYRK homology (DH) box, an aspartic rich sequence that precedes the kinase domain (Becker & Joost, 1999), a characteristic HCD motif in the catalytic loop, instead of the highly conserved HRD (Kannan & Neuwald, 2004), and a YxY motif with the second tyrosine being auto-phosphorylated and required for DYRK activity (Lochhead *et al.*, 2005). Regulatory sequences including nuclear localisation sequences (NLSs) and a PEST sequence known to act as signal for protein degradation., are present in specific members of the DYRK family (Aranda *et al.*, 2011).

Recently, a role in differentiation was shown for a DYRK related kinase of the trypanosomatid parasite *Trypanosoma brucei*. Mony *et al* performed a genome-wide RNAi target screen to identify genes whose down-regulation resulted in a cAMP unresponsive phenotype (Mony *et al.*, 2014). This phenotype was associated with a differentiation defect, whereby parasites failed to differentiate from the "proliferative slender" to the "arrested stumpy" form, the latter stage being responsible for transmission to the tsetse flies (Mony *et al.*, 2014). In addition, another DYRK member from *T. brucei* has been shown to be required for parasite survival in the mouse (Fernandez-Cortes *et al.*, 2017).

Interestingly, in *Leishmania* the DYRK family consists of 8 members. DYRK1 homologue (*LinJ*.15.0180, *Lin*DYRK1) is a single-copy gene which is a *Leishmania* DYRK1 homologue having the highest conservation to mammalian DYRK1A and DYRK1B orthologues. Herein, we combined genetic manipulation and phenotypic analyses to generate null mutants and report that *Lin*DYRK1 is a pro-survival kinase and its deletion is associated with a deregulated stationary phase biology.

Results

Evolutionary relationship and characterisation of *Leishmania* DYRK family members

To investigate the identity and evolutionary relationship of *Leishmania* DYRK family proteins, we employed phylogenetic analyses of animal, plant, insect, yeast and protist DYRK protein sequences. Our analysis revealed the presence of 8 *Leishmania* DYRK proteins, in accordance to previous reports (Parsons *et al.*, 2005). From the *Leishmania* DYRK members, five belong to all three DYRK subfamily groups, namely the DYRK (*Lin*J.15.0180-*Lin*DYRK1, *Lin*J.14.0890 and *Lin*J.33.1930), the HIPK (*Lin*J.19.0360) and the Prp4 (*Lin*.J.36.4460) **(Fig 1A**). The other three

family members (*Lin*J.21.2010, *Lin*J.14.1140 and *Lin*J.35.1850) did not cluster with the known DYRK subfamilies (**Fig 1A**).

*Lin*DYRK1 possesses sequences, including the HCD triplet in the catalytic loop and a Tyrosine (HRY^{523}), aligning to the second tyrosine of the DYRK subfamily activation loop sequence YxY that conform to DYRK constraints (**Fig 1B**, **S1 Fig**). In addition, *Lin*DYRK1 is more similar to mammalian DYRKs than to lower eukaryotic YAKs (**S1 Fig**). For example, *Lin*DYRK1 is closer in sequence identity to *H. sapiens* (*Hs*) DYRK1A (48.5% identity, query cover 97%, E value: 1*e^{-63}) and *Hs*DYRK1B (49.5%, query cover: 96%, E value: 4*e^{-65}), than to *S. cerevisiae* Yak1p (46.55% identity, query cover 59%, E value: 1*e^{-35}).

In *Leishmania,* the kinase with the highest similarity to *Lin*DYRK1 is *Lin*J.14.0890 (**Fig. 1B**). The full protein sequences share an overall 54% sequence identity (54% query cover, E value: 8e-74), while both proteins have a long N terminal domain of unknown function, unique to *Leishmania*. The two kinases lack a NLS and contain predicted PEST sequences (**Fig 1B**). The DH box, while conserved in *Lin*DYRK1, is not present in *Lin*J.14.0890, whereas *Lin*J.14.0890 also possesses a conserved tyrosine (PKY^{743}), in its predicted activation loop. This kinase however, has insertions in the activation loop between subdomains VII and VIII and between subdomains X and XI (**Fig 1B**), and thus its catalytic activity merits experimental validation.

Apart from *Lin*J.14.0890, other *Leishmania* DYRK family members have important modifications of consensus sequences within the kinase domain. For example, *Lin*J.21.2010 and *Lin*J.14.1140 are characterised by the atypical glycine rich loops DXAXXSXXV and GXAXXSXXV respectively, that replace the highly conserved GXGXXGXV required for the positioning of ATP (**S2 Fig**). Interestingly, *Lin*J.19.0360 contains an atypical DFS cation binding site instead of the highly conserved DF/LG (**S2 Fig**) and thus the catalytic activities of these kinases require confirmation.

*Lin*DYRK1 localisation

To investigate the subcellular localisation of *Lin*DYRK1, we expressed a tagged version of *Lin*DYRK1 with eGFP at its N-terminus (GFP-*Lin*DYRK1) from an episome. In logarithmic cultures, *Lin*DYRK1-GFP was mainly localised at the anterior side of the cell. Co-localisation with mitotracker was used in an attempt to compare *Lin*DYRK1 localisation in logarithmic cells with respect to the mitochondrion. Our results showed that GFP-*Lin*DYRK1 in logarithmic cells, exhibited no co-localisation with mitotracker (**Fig 2A**). Moreover, concanavalin A (ConA) conjugated to Alexa594 (ConA–Alexa594) used to label the surface glycocalyx and the flagellar pocket (Ilgoutz *et al.*, 1999), revealed that GFP-*Lin*DYRK1 occupied a portion of the flagellar pocket area (**Fig 2B**). GFP-*Lin*DYRK1 was also found outside the flagellar pocket at the anterior end of the kinetoplast (**Fig 2B**) and between the nucleus and kinetoplast (**Fig 2A** and **Fig 2B**). In order to further investigate the localisation of *Lin*DYRK1 in logarithmic cells, FM4-64 dye was used as a marker of endosomes (Besteiro *et al.*, 2006). Areas of intense localisation of GFP-*Lin*DYRK1 were observed, similar to the localisation of FM4-64, in a 3 min pulse chase experiment followed by an incubation time of 20 min incubation at RT **(Fig 2C)**. GFP-*Lin*DYRK1 in late logarithmic/ early stationary phase promastigotes extended more throughout the cell body (**Fig 2A**) but showed a distinct localisation with respect to mitotracker (**Fig 2A**). In late (stationary phase day 7 of cell culture, day 3 of stationary phase) however, we observed a change in GFP-*Lin*DYRK1 localisation to areas, where mitotracker was present (**Fig 2A**).

To ensure that the observed *Lin*DYRK1 localisation was not an artefact, we expressed from an episome a second fusion protein, tagged with eGFP at its C-terminus (*Lin*DYRK1-GFP). *Lin*DYRK1-GFP had a similar localisation to GFP- *Lin*DYRK1 (**S3A** and **S3B Fig**). Despite the fact that episomal expression can sometimes cause excessive expression of the target protein, that might result in potential mislocalisation (Tanz *et al.*, 2013), this does not seem to be the case in our system. The levels of N and C terminal tagged fusion proteins were much lower than GFP, and below the detection limit by western blot analysis in total protein extracts (data not shown).

In addition, the fact that similar localisation for both C and N terminal fusion proteins was observed, is a strong indication that they represent the localisation of the endogenous protein.

*Lin*DYRK1 over-expression has a negative effect on promastigote growth

To have a better understanding of the *Lin*DYRK1 function, we created a *L. infantum* cell line that over-expresses the protein from a *Leishmania* expression plasmid (pXNG4). This plasmid expresses Herpes Virus Thymidine kinase (HSV-TK) and can be subject to negative selection by antiviral drug gancinclovir (GCV), which is phosphorylated by HSV-TK into a toxic product (Murta *et al.*, 2009). Parasites over-expressing *Lin*DYRK1 {*Lin*DYRK1$^{+/+}$[pXNG-*Lin*DYRK1]} had a proliferation defect with respect to control parasites {wild type (*Lin*DYRK1$^{+/+}$), parasites that had lost the episome after treatment with GCV {*Lin*DYRK1$^{+/+}$[pXNG-*Lin*DYRK1]} and parasites transfected with plasmid alone {*Lin*DYRK1+/+[pXNG]} visible at seeding density of 10^6 mL^{-1} **(Fig 3A)**. In order to measure more precisely the growth defect, a lower seeding density was used (3 *10^5 mL^{-1}) for *Lin*DYRK1$^{+/+}$[pXNG-*Lin*DYRK1] and *Lin*DYRK1$^{+/+}$[pXNG] promastigotes. The logarithmic slopes of the growth curves were compared and our results demonstrated that *Lin*DYRK1 over-expressing parasites proliferated 33% less well than parasites bearing plasmid alone **(Fig 3A)**. Cell cycle progression of *Lin*DYRK1 over-expressing parasites was also investigated by initially synchronising *Lin*DYRK1$^{+/+}$[pXNG-*Lin*DYRK1] and *Lin*DYRK1$^{+/+}$[pXNG] promastigotes at the G_0/G_1-S boundary with an inhibitor of ribonucleotide reductase, hydroxyurea (HU). Subsequently cell cycle re-entry was allowed by removal of HU. Cell cycle was investigated 0 h, 3 h and 6.5 h after HU removal. At 6.5 h post HU removal 51% of *Lin*DYRK1$^{+/+}$[pXNG-*Lin*DYRK1] parasites had not entered in S-G2/M phases in contrast to only 15% of control *Lin*DYRK1$^{+/+}$[pXNG] parasites (**Fig 3B, S1 Table**), and revealed that *Lin*DYRK1 over-expression resulted in delayed cell cycle re-entry of resting cells.

*Lin*DYRK1 gene deletion is tolerated in logarithmic phase promastigotes

Assuming initially that *Lin*DYRK1 was essential, we decided to generate *Lin*DYRK1 facilitated knockouts, a process that overcomes a potentially lethal phenotype (Dacher *et al.*, 2014, Murta *et al.*, 2009). The episome [pXNG4] mentioned above, also expresses GFP, which is used as a reporter for monitoring its loss (Dacher *et al.*, 2014, Murta *et al.*, 2009). By sequentially introducing the puromycin N-acetyl-transferase (PAC) and then the hygromycin B (HYG) targeting cassettes, we replaced the two *Lin*DYRK1 alleles in *L. infantum* promastigotes transfected with [pXNG-*Lin*DYRK1] (**S4A Fig**). Following this strategy, we generated two homozygous facilitated mutants from two independent heterozygous clones (**A** and **B**). We confirmed incorporation of the targeting of cassettes into the *Lin*DYRK1 genomic locus by diagnostic PCR (**S4B Fig**).

We then tested if *Lin*DYRK1 was essential for promastigote survival. To this end, we applied negative selection by replacing the positive selection drug NTC with the negative selection drug GCV and analysed the loss of the episome by measuring the GFP fluorescence by flow cytometry. Analysis of the GFP fluorescence of both clones **A** and **B** for 4 passages in logarithmic phase revealed that the *Lin*DYRK1 expressing episome could be eliminated after the addition of GCV, in a similar manner to the episome in wild type promastigotes (**Fig. 4A**). Moreover, the mean GFP fluorescence gradually was reduced to similar levels of wild type *Lin*DYRK1$^{+/+}$ promastigotes (**Fig 4B**). To be certain that the loss of fluorescence in the pools of parasites correlated with the loss of the [pXNG-*Lin*DYRK1] episome, we analysed by western blotting the GFP amounts of individual clones isolated after 15 passages of cell-culture, using alpha-tubulin as a loading control (**Fig 4C**). We did not observe GFP expression in any of the clones tested (**Fig 4C**), revealing that *Lin*DYRK1$^{-/-}$ parasites can be viable without the episome, while GFP was detected in the control *Lin*DYRK1$^{+/+}$[pXNG-*Lin*DYRK1] pool treated with NTC (**Fig 4C**). To rule out the possibility of an extra copy of *Lin*DYRK1 anywhere within the genome of *L. infantum*, we performed diagnostic PCR with internal *Lin*DYRK1 primers (p1 and p2) in

selected clones after GCV selection, and failed to amplify a product (**S4C Fig**). Overall, our findings showed that the loss of the [pXNG-*Lin*DYRK1] episome could be tolerated in logarithmic cells and that *Lin*DYRK1 is not essential for viability.

The experiment was also repeated without the presence of the episome, in order to ascertain that GCV does not alter the phenotype of these cells. We were able to generate and *Lin*DYRK1$^{-/-}$ promastigotes, termed here direct heterozygous *Lin*DYRK1$^{+/-direct}$ and direct homozygous *Lin*DYRK1$^{-/-direct}$ mutants. Correct incorporation of targeting cassettes and lack of internal *Lin*DYRK1 copy were validated by PCR (**S4D Fig**).

*Lin*DYRK1 deletion affects stationary growth phase

To further investigate the biological role of *Lin*DYRK1, we analysed some phenotypes of *Lin*DYRK1$^{-/-}$ parasites, including growth comparisons. In the logarithmic phase clones *Lin*DYRK1$^{-/-}$**B1** and *Lin*DYRK1$^{-/-}$**B2** displayed a higher proliferation rate (40% and 66% for clones **B1** and **B2** respectively) and higher maximal cell density than their parental cell line *Lin*DYRK1$^{-/-}$[pXNG-*Lin*DYRK1]**B** (**S5A Fig**). A higher proliferation was also observed for *Lin*DYRK1$^{-/-}$**A1** and *Lin*DYRK1$^{-/-}$**A2** clones with respect to their parental line (data not shown). In addition, growth comparison between a *Lin*DYRK1**A1**$^{-/-}$ add back cell line and *Lin*DYRK1**A1**$^{-/-}$ promastigotes transfected with plasmid alone {*Lin*DYRK1$^{-/-}$[pXNG]}, revealed that add backs displayed 30% reduced proliferation rate and lower maximal cell density (**S5B Fig**). Moreover, the homozygous *Lin*DYRK1$^{-/-direct}$ also proliferated better than the heterozygous *Lin*DYRK1$^{+/-direct}$ **(S5C Fig**). These results altogether, allow us to conclude that the lack of *Lin*DYRK1 has a positive effect on the growth rate of logarithmic cells.

Despite the fitness of *Lin*DYRK1$^{-/-}$ mutants in logarithmic growth phase, in stationary phase these cells displayed defects including morphological alterations. All experiments in stationary growth phase, were performed the second day of stationary growth phase, unless stated otherwise. Stationary *Lin*DYRK1$^{-/-}$ parasites, were less elongated, had greater width and were

more rounded than wild type, parental *Lin*DYRK1$^{-/-}$[pXNG-*Lin*DYRK1] lines and an add back clone (**Fig 5A**). Similar morphological alterations were observed with direct null mutants (**S6A Fig**). Flow cytometry analysis confirmed these findings which showed higher forward scatter (FSC) values for both facilitated *Lin*DYRK1$^{-/-}$ **(S6B Fig)** and the *Lin*DYRK1$^{-/-direct}$ mutants **(S6C Fig)** in comparison to control promastigotes. Moreover, null mutants in stationary phase accumulated a greater percentage of cells with two nuclei (N) and two kinetoplasts (K) (17% and 29% of clones *Lin*DYRK1$^{-/-}$**A1** and *Lin*DYRK1$^{-/-}$**A2**, respectively), and a greater percentage of cells with 2N1K (7% and 12.5% for clones *Lin*DYRK1$^{-/-}$**A1** and *Lin*DYRK1$^{-/-}$**A2**, respectively) versus ≤3.3% of 2N2K and ≤1% of 2N1K of control cells (parental line *Lin*DYRK1$^{-/-}$[pXNG-*Lin*DYRK1]**A** and *Lin*DYRK1$^{+/+}$) (**S6D Fig**). This could be an indication that these promastigotes are in a stress related G_2/M cell cycle arrest, which in due time results in cell death (Azzopardi *et al.*, 2017).

Cell death was increased in late stationary phase in facilitated and direct *Lin*DYRK1$^{-/-}$ clones (**Fig 5B**, **S7 Fig, Table S2A**). For facilitated clones *Lin*DYRK1$^{-/-}$**A1** and *Lin*DYRK1$^{-/-}$**A2**, 46.3% and 33.8% respectively had hypodiploid DNA content, versus 4.9% of wild type *Lin*DYRK1$^{+/+}$, 15.2% of *Lin*DYRK1$^{-/-}$ [pXNG-*Lin*DYRK1]**A** and 9% of *Lin*DYRK1$^{-/-}$**A1**[pXNG-*Lin*DYRK1] add back (**Fig 5B, Table S2A**). In early stationary phase (day 5 of growth curve, day 1 of stationary phase) *Lin*DYRK1$^{-/-}$ mutants did not show increase of hypodiploid DNA content (**S7A Fig),** whereas late stationary phase (day 7 of growth curve, day 3 of stationary phase).

*Lin*DYRK1$^{-/-}$ stationary phase promastigotes exhibit severe surface aberrations, lipid body formation and display notable lipid content changes

To further investigate the morphological defects of *Lin*DYRK1$^{-/-}$ parasites in stationary phase, we performed scanning (SEM) and transmission (TEM) electron microscopy SEM analysis of facilitated *Lin*DYRK1$^{-/-}$ mutants revealed had surface aberrations, with folds on the surface and membrane invaginations (**Fig 6A**). TEM analysis revealed that *Lin*DYRK1$^{-/-}$

promastigotes displayed an abnormal subcellular structure. These parasites exhibited intense vacuolisation of the cytoplasm, (**Fig 6B**{III, IV, V, VI}). Vacuoles often contained membrane blebs, where the kinetoplast membrane dissociated inside a vacuole (**Fig. 6B**{V}). Another prominent ultrastructural feature of *Lin*DYRK1$^{-/-}$ parasites was the presence of lipid vacuoles or bodies observed by their low electron density and homogeneous appearance (Charron & Sibley, 2002). Lipid bodies were found to be adjacent to vacuoles and often were merging with the cell membrane, leaving an open invagination full of lipids (**Fig. 6B** {III and IV}). In addition some parasites had fragmented DNA **(Fig. 6B** IV), suggesting that they were already in the process of cell death.

As lipid droplet formation may be linked to lipid metabolism (Walther & Farese, 2012), we further investigated the lipid composition of *Lin*DYRK1$^{-/-}$ promastigotes. To this end, we analysed the total phospholipid content by nano-electrospray mass spectrometry (nESI-MS), and by gas chromatography mass spectrometry (GC-MS) the total fatty acid and sterol content. We analysed two knockout clones *Lin*DYRK1$^{-/-}$**A** and *Lin*DYRK1$^{-/-}$**B** from different parental strains to normalise for colony specific effects, and compared them with wild type parasites (*Lin*DYRK1$^{+/+}$) and the parental clone *Lin*DYRK1$^{-/-}$[pXNG-*Lin*DYRK1] **A**. Our results showed that *Lin*DYRK1 mutants had higher amounts of saturated fatty acids (**Fig. 6C**, **Table 1**). The most evident difference was a decrease in the percentage of 18:2, and an increase in that of 18:0 (**Table 1**), resulting in a C18:2/C18:0 fatty acid ratio of ~0.7 and ~0.8 for the clones *Lin*DYRK1$^{-/-}$**A1** and *Lin*DYRK1$^{-/-}$**B1** respectively, versus 1.7 for wild type cells. Furthermore, sterol analysis showed that *Lin*DYRK1$^{-/-}$parasites displayed relatively lower cholesterol levels than the pool of *Lin*DYRK1$^{+/+}$ parasites (14-15% mutants versus 27% wild type) and higher ergosta-7,24-dien-3β-ol levels (17.8%-22% mutants versus 11% wild type) (**Table 1**). Finally, our analysis demonstrated that *Lin*DYRK1 knockout does not significantly affect phospholipid composition (**S8 Fig**).

*Lin*DYRK1$^{-/-}$ promastigotes exhibit defects in markers of infective promastigotes, increased thermosensitivity and reduced survival in host macrophages

To ensure survival within the mammalian host, *Leishmania* promastigotes develop resistance to complement-mediated lysis, as they progress from the logarithmic to stationary growth phase (Franke *et al.*, 1985). In an attempt to relate *Lin*DYRK1$^{-/-}$ stationary phase defects with parasite infectivity, the ability of null mutants to endure complement lysis in logarithmic and stationary phase was assessed. *Lin*DYRK1$^{-/-}$ promastigotes were more susceptible to complement lysis (70% logarithmic and 30% stationary phase) than *Lin*DYRK1$^{+/+}$ (46.7% logarithmic and 17.8% stationary phase) and *Lin*DYRK1$^{-/-}$[pXNG-*Lin*DYRK1] (53% logarithmic and 16.5 % stationary phase) promastigotes (**Fig 7A**).

The number of infective metacyclics and the expression of metacyclic enriched transcripts were also measured for stationary phase *Lin*DYRK1$^{-/-}$ mutants and control cells. For measuring metacyclics, the peanut agglutinin (PNA) assay was performed, which relies on the ability of the PNA lectin to bind and agglutinate non-infective procyclics but not infective metacyclic promastigotes (Sacks *et al.*, 1985). The assay revealed that that the percentage of unagglutinated *Lin*DYRK1$^{-/-}$ parasites was 2.8 times less than wild type *Lin*DYRK1^{+}/$^{+}$ and 3.6 times less than *Lin*DYRK1$^{-/-}$[pXNG-*Lin*DYRK1] (**Fig 7B**). In addition, *Lin*DYRK1$^{-/-}$ parasites expressed less well transcripts known to be enriched in metacyclic promastigotes. More specifically levels of prohibitin {*Lin*J.16.1710 (Almeida *et al.*, 2004)}, meta1 {*Lin*J.17.0990, (Nourbakhsh *et al.*, 1996)} and HASPB {*Lin*J23.1220} (Sadlova *et al.*, 2010)} transcripts normalised with ribosomal protein S29 transcript (*Lin*J.28.2360) were compared. The ratios of normalised transcripts were significantly reduced with respect to wild type *Lin*DYRK1$^{-/-}$ **A1** (7.14 fold less for prohibitin, 5 fold less for meta1 and 4.17 fold less for HASPB) and to *Lin*DYRK1$^{-/-}$ [pXNG-*Lin*DYRK1]**A** (2.57 fold less for prohibitin, 2.6 fold less for meta1and 1.46 less for

HASPB) (**Fig. 7C**). These results suggest that stationary phase defects are not only morphological in *Lin*DYRK1-/- but also biochemical, and are consistent with defects in metacyclogenesis.

In addition to metacyclogenesis, other factors may influence stage differentiation as the ability to survive a 26→37^{o}C upshift in temperature, which mimics the sand-fly to mammalian host temperature transition. As DYRK related kinases are known to regulate thermotolerance (Hartley *et al.*, 1994), we hypothesised that *Lin*DYRK1$^{-/-}$ promastigotes were less thermotolerant. We subjected parasites to a 16 h 26→37^{o}C heat-shock and compared the percentage of hypodiploid cells in facilitated (**Fig 7D**, **S2C Table**) and direct mutants (**S2D Table, S6 Fig**) with the corresponding control cells. Our analyses showed that all *Lin*DYRK1 knockouts were more sensitive to heat-shock than control cell lines **(Fig 7D**, **S7 Fig, S2C&D Table**). More specifically 28% and 29% of *Lin*DYRK1$^{-/-}$ clones **A1** and **A2** had hypodiploid DNA content, versus 17.1% of the parental strain, 16.12% of the *Lin*DYRK1$^{-/-}$[pXNG-*Lin*DYRK1] add back and 12.5% of the wild type *Lin*DYRK1$^{+/+}$ promastigotes **(Fig 7D**, **S2C&D Table**). Comparison of direct mutants also confirmed that lack of *Lin*DYRK1 gave rise to a more thermosensitive phenotype **(S9 Fig**, **S2C&D Table**), reinforcing that heat shock sensitivity is specifically related to loss of *Lin*DYRK1 expression.

We then performed an *in vitro* infection assay and compared the percentage of infection and survival of *Lin*DYRK1$^{-/-}$, *Lin*DYRK1$^{-/-}$[pXNG-*Lin*DYRK1] and *Lin*DYRK1$^{+/+}$ stationary phase parasites in murine peritoneal macrophages. The infection rate of *Lin*DYRK1$^{-/-}$ parasites (% of infected macrophages and number of parasites per macrophage) was dramatically reduced by 10.5-fold (2.7 less % infected macrophages and 3.9 times less parasites per macrophage) 72 h post infection, compared the beginning of infection (**Fig 7E**). The controls, *Lin*DYRK1$^{+/+}$ and *Lin*DYRK1$^{-/-}$[pXNG-*Lin*DYRK1], presented similar rates or moderate reduction of infection rates 72 h post infection compared to the beginning of infection (**Fig 7E**). In addition, we attempted to measure the *in vivo* infectivity of these parasites. To this end, efforts were made to recover freshly isolated wild type and transgenic parasites cultivated in parallel, from livers of BALB/c mice.

During these attempts, it was possible to recover only *Lin*DYRK1$^{-/-}$ [pXNG-*Lin*DYRK1] parasites in one of the three mice used per group. Parasite burden of animals infected was measured two weeks post-infection by qPCR using liver DNA to estimate the amount of the *Leishmania* specific arginine permease gene AAP3 (Tellevik *et al.,* 2014) and corresponded to 1530 parasites per 8700 hepatocyte nuclei. This result is suggestive of the reduced ability of *Lin*DYRK1$^{-/-}$ promastigotes to survive in mice, as the ability of parasites to survive in mice is compromised even in wild type background parasites due to the continuous cultivations and manipulations.

Discussion

In this work, we determined the evolutionary relationship of the *Leishmania* DYRK family members. A clustering of *Leishmania* DYRK family members both within (for 5 out of 8), and outside (for 3 out of 8) of the known subfamilies (DYRKs, HIPKs, Prp4s), suggests that the DYRK taxonomy in its current form, requires revisiting and the inclusion of a more representative repertoire of eukaryotic organisms. Differences in highly conserved sequences (glycine rich loop, cation binding site) of the kinase catalytic domain for specific *Leishmania* DYRK family members indicate that these are either pseudokinases or kinases with atypical features mirroring the unique biology of the parasite. *Lin*DYRK1 is one of the genes that shares all the features of an active kinase, and recombinant *Lin*DYRK1 has been shown to be an active kinase (Hombach-Barrigah *et al.,* 2019).

*Lin*DYRK1 had a distinct localisation in logarithmic, stationary and late stationary growth phases. *Lin*DYRK1 localisation in proliferative and early stationary phases, in the flagellar pocket area, a structure known to carry out endo- and exo-cytosis (Stierhof *et al.,* 1994) and endosomes involved in endocytic cycle (Besteiro *et al.,* 2006) and mitochondrial localisation in late stationary phase, show that *Lin*DYRK1 signaling is growth stage dependent. The

endosomal localisation data is reminiscent of a known role for mammalian DYRK1A in endocytosis and vesicle recycling (Murakami *et al.*, 2009, Murakami *et al.*, 2012).

In this study, it was shown that *Lin*DYRK1 knockouts were viable and that in the logarithmic growth phase had a higher proliferation rate than control cell lines. At the same time, over-expression of *Lin*DYRK1 in *Leishmania* resulted in decreased proliferation and delayed cell cycle re-entry after synchronisation by HU. These results could be in line with the known role of DYRKs in various cell types, in regulating the decision between cell cycle re-entry and cell cycle exit (Soppa & Becker, 2015) in mitogen-poor environments (Becker, 2018, Garrett & Broach, 1989). In *Leishmania* however, further enquiry is needed to address if there is a direct role for *Lin*DYRK1 in cell cycle control and proliferation, including the identification of partners and substrates.

One of the most prominent phenotypes observed in this study was the deregulated phenotype of stationary phase *Lin*DYRK1$^{-/-}$ mutants. Stationary phase phenotypes in unicellular organisms are known to have activated the internal systems of protection against stress and are able to survive better under adverse or changing environmental settings (Pletnev *et al.*, 2015). In *Leishmania* too, stationary phase promastigotes have increased ability to survive in the intracellular environment of the mammalian host (Wozencraft & Blackwell, 1987) and this ability is associated with metacyclogenesis (da Silva & Sacks, 1987). In our system *Lin*DYRK1$^{-/-}$ stationary phase promastigotes displayed several defects. Knockout parasites were more round and exhibited an intense vacuolisation of the cytoplasm. The formation of vacuoles in wild type cells could be the result of an ongoing autophagic process, a survival process (Smirlis *et al.*, 2010) that also occurs during the procyclic to metacyclic promastigote stage differentiation (Williams *et al.*, 2006). Prolonged, autophagy results in cell death (Smirlis *et al.*, 2010), and could explain the cell death observed in long range stationary phase promastigotes.

The accumulation of lipid bodies and the switch in the ratio of saturated (18:0) and polyunsaturated (18:2) fatty acids in stationary phase *Lin*DYRK1$^{-/-}$ promastigotes, may be related

to the formation of lipid bodies, as this switch of identical lipids in mammalian cells corroborates to the formation of large lipid droplets (Arisawa *et al.*, 2016). Most importantly, large lipid droplets are induced by stress (Petan *et al.*, 2018), while changes in relative ratios of saturated fatty acids are anticipated in normal procyclic to metacyclic stage differentiation (Silva *et al.*, 2011). Hence our results suggest abnormal differentiation processes and/or stress response. Sterol metabolism is also known to be affected differentially in *Leishmania* logarithmic and stationary phase cultures (Jacobs *et al.*, 1982). The decrease observed for the relative amount of cholesterol in *Lin*DYRK1$^{-/-}$ parasites, is suggestive of a disruption in uptake. This is less explainable for the parent cell line *Lin*DYRK1$^{-/-}$[pXNG-*Lin*DYRK1] but even in these cells some vacuolisation is visible. Conversely, the alteration in sterol composition may be entirely due to upregulation of the synthesis of some of endogenous ergostane-based sterols, clearly visible in the putative terminal molecule of the pathway, ergosta-7,24-dien-3β-ol (Yao & Wilson, 2016).

In addition, defects in metacyclogenesis, infectivity and thermotolerance of *Lin*DYRK1$^{-/-}$ parasites mirror the importance of the kinase in the completion of the *Leishmania* life-cycle. The enrichment of the *S. cerevisiae* YAK1 in differentiated quiescent yeast stationary-phase cultures (Aragon *et al.*, 2008) and its thermoprotective function in yeast (Hartley *et al.*, 1994), may reveal a central role of DYRK kinases in stationary phase biology and thermoprotection.

Overall, our findings suggest that *Lin*DYRK1 signalling is needed to normal promastigote development. This finding is one step further for gaining insight into the contribution of protein phosphorylation in the growth-stress response balance, and it opens new areas of research and future challenges, including search of DYRK1 substrates the role *Lin*DYRK1 in the amastigote stage.

Experimental Procedures

Multiple sequence alignment

To search DYRK kinases in *Leishmania*, BLAST analysis was performed with blastp algorithm using protein sequences of known DYRK genes from *H. sapiens*, *D. melanogaster*, *S. cerevisiae* as queries. Sequences from *L. infantum*, *T. cruzi* and *T. brucei* were retrieved from the NCBI (http://www.ncbi.nlm.nih.gov/protein/) and TriTrypDB databases (http://tritrypdb.org/tritrypdb/). Protein alignment was performed using CLUSTALW 2.0.12 using the built-in programs (Bioedit). Unrooted phylogenetic tree defined by amino acid sequence similarities was generated using Interactive Tree of Life (http://itol.embl.de/). Sequence accession numbers are shown in **S3 Table**.

Plasmids

For the generation of [pXNG-*Lin*DYRK1] construct, the open reading frame (ORF) of *Lin*DYRK1 (*Lin*J.15.0180) was amplified by polymerase chain reaction (PCR) from *L. infantum* (L4, MHOM/GR/78/L4) genomic DNA and cloned into the *Leishmania* expression plasmid [pXNG4]. To this end, the p1/p2 primer pair (**S4 Table**) were used and *Lin*DYRK1 ORF was cloned into the BglII (New England Biolabs) site of [pXNG4] plasmid.

*Lin*DYRK1 targeting constructs, encoding for HYG and PAC resistance markers to antibiotics hygromycin B and puromycin respectively, flanked by the ~ 900 bp 5' and 3' UTR of the Lin*DYRK1* gene, were generated for replacing the genomic *Lin*DYRK1 ORF. To this end, the 900 bp 5'-UTR and 3'-UTR of *Lin*DYRK1were PCR-amplified using primer pairs p3/p4 and p5/p6, respectively (**S4 Table**), and cloned by TA cloning in the appropriate orientation into [pGEM-T] and [pGEM-T Easy] vectors (Promega) respectively, resulting in pGEM-5'UTR and [pGEM-T Easy-$^{3'}$UTR] plasmids. The *Lin*DYRK1 3'UTR was released using NotI restriction enzyme (New England Biolabs) and cloned into the NotI site of pGEM-5'UTR in the appropriate orientation, to generate plasmid [pGEM-5'UTR-3'UTR]. HYG and PAC coding sequences were PCR-amplified from plasmids [pX63-Hyg] and [pXG-PAC], using primer pairs p7/p8 and p9/p10

and cloned into the SpeI/BamHI restriction sites of [pGEM-5'UTR-3'UTR]. Primers p3 and p6 also contained an internal PmeI (**S4 Table**) restriction site, which was used for the generation of linear constructs prior to electroporation.

To generate a GFP-*Lin*DYRK1 fusion construct, the *Lin*DYRK1 insert was sub-cloned from [pXNG-*Lin*DYRK1] in the BglII site of [pXG-GFP^{+2}] plasmid. To generate the [*Lin*DYRK1-GFP] fusion construct, the *Lin*DYRK1 insert encoding the ORF was amplified by PCR from genomic *L. infantum* (L4, MHOM/GR/78/L4) DNA with the use of the p1/p21 primer pair (**S4 Table**). The PCR product was digested with BglII and BamHI and inserted in the appropriate orientation in the BamHI site of [PXG-PAC] *Leishmania* expression plasmid to generate plasmid [*Lin*DYRK1-carboxyterminal]. The eGFP was PCR amplified from [pEGFP(N3)] (Clontech®) using the p22/ p23 primers pair (**S4 Table**), digested with BamHI and BglII. The product was cloned in the appropriate orientation in the BamHI site of plasmid [*Lin*DYRK1-carboxyterminal], to generate plasmid [pXG-PAC-*Lin*DYRK1-GFP]. All constructs were confirmed by sequencing.

Cell culture and transfection

L. infantum L4 strain (L4, MHOM/GR/78/L4) promastigotes were cultivated at 26° C in M199 medium supplemented with 10% foetal bovine serum, 100 µM adenine, 10 µg mL^{-1} hemin, 40 mM HEPES (N-2-hydroxyethylpiperazine-N'-2-ethanesulfonic and acid) (pH 7.4), and 50 units of Penicillin-Streptomycin (Gibco Laboratories) (Kapler *et al.*, 1990) and *L. amazonensis* parasites (MHOM/BR88/BA-125, Leila strain) were cultured in cultured in Schneider's insect medium (Sigma Aldrich, St. Louis, MO) supplemented with 10% fetal bovine serum (Gibco Laboratories, Gaithersburg, MD).

Parasite transfection was performed in logarithmic phase promastigotes that were washed in electroporation buffer (21 mM HEPES pH 7.5, 137 mM NaCl, 5 mM KCl, 0.7 mM Na_2HP0_4 and 6 mM glucose) and transfected by electroporation with 20 µg of plasmids DNA ([pXNG-

*Lin*DYRK1] , pXG-GFP-*Lin*DYRK1] or [pXG-PAC-*Lin*DYRK1-GFP]), according to previously established protocols (Beverley & Clayton, 1993). Parasites transfected with [pXNG-*Lin*DYRK1] and [pXGGFP^{+2}-*Lin*DYRK1] constructs were selected in fully supplemented culture medium in the presence of 150 μg mL^{-1} NTC, 50 μg mL^{-1} G418 and 30 μg mL^{-1} puromycin, respectively.

For the generation of *Lin*DYRK1 facilitated mutants, we followed the methodology described (Dacher *et al.*, 2014). More specifically, *Lin*DYRK1$^{+/+}$[pXNG-*Lin*DYRK1] *L. infantum* promastigotes were first transfected with 3 μg of PmeI linearised and dephosphorylated PAC targeting cassette. Parasites were plated 12 h post transfection in solid medium (fully supplemented M199 containing 1% (w/v) noble agar, 60 μg mL^{-1} puromycin and 100 μg mL^{-1} NTC. Two independent clones were selected to check for correct PAC cassette genomic integration. Integration was validated by PCR using genomic DNA of the two colonies as template and primers p14/p11 (**S4 Table**). After the confirmation of the cassette replacement into the DYRK1 genomic locus, two independent *Lin*DYRK1$^{+/-}$[pXNG-*Lin*DYRK1] heterozygous clones **A** and **B**, were transfected with 3μg of PmeI linearised and dephosphorylated HYG targeting cassette and selected in solid medium (see above), which contained 60 μg mL^{-1} puromycin, 60 μg mL^{-1} hygromycin B and 100 μg mL^{-1} NTC. Representative homozygous clones derived from both **A** and **B** heterozygous clones were selected and analysed for the correct integration of the HYG replacement cassette and the absence of genomic *Lin*DYRK1 ORF with the primer pairs p14/p12 and p14/p13, respectively (**S4 Table**). For generating "direct knockouts", the same procedure was performed in wild type cells that had not been previously transfected with the construct [pXNG-*Lin*DYRK1].

To negatively select against [pXNG-*Lin*DYRK1], the NTC antibiotic was replaced by 50 μg mL^{-1} of GCV in *Lin*DYRK1$^{-/-}$[pXNG-*Lin*DYRK1] and *Lin*DYRK1$^{+/+}$[pXNG-*Lin*DYRK1] parasites, used as control, as previously described (Dacher *et al.*, 2014). For passive loss of the [pXNG-*Lin*DYRK1] episome, the NTC antibiotic was omitted from the culture medium. For selecting single colonies parasites were plated on M199 agar plates (Dacher *et al.*, 2014).

Promastigote growth was assessed microscopically by counting fixed cells daily in a malassez cell-counting chamber or by flow cytometry. All growth curve experiments were performed at least three times.

SDS-polyacrylamide gel electrophoresis (SDS-PAGE) and immunoblotting

SDS-polyacrylamide gel electrophoresis (SDS-PAGE) was performed by the method of Laemmli (Laemmli, 1970). For immunoblotting, proteins were transferred on a nitrocellulose filter (Hybond C, Amersham Biosciences) and immunoblotting was performed as previously described (Papageorgiou & Soteriadou, 2002). For the analysis of GFP expression, we performed immunoblotting using monoclonal mouse antibodies anti-GFP (Miltenyi) and mouse anti-α tubulin (Sigma), both at 1:2000 dilution. A mouse horseradish peroxidase-conjugated antibody (Pierce) was finally added, and the image acquired by ECL® Plus (enhanced chemiluminescence) (GE Healthcare), according to the manufacturer's instructions. After the development of the first signal corresponding to GFP, the blots were stripped and reprobed with anti-tubulin antibody.

Flow cytometry

For measuring the GFP fluorescence of live parasites, parasites were incubated with 50 μg mL^{-1} propidium iodide (PI). GFP was analysed in the FL1 channel or 525/40 BP filter and PI in FL2 or 610/20 BP of FACS Calibur (Becton Dickinson) and Cytoflex 5 (Beckman Coulter), respectively. For cell cycle analysis, logarithmic parasites were synchronised in the G_1/S boundary with 2.5 mM of HU (Sigma Aldrich) for 12 h, as previously reported. The DNA content of promastigotes was analysed by PI staining of RNAse A treated and ethanol fixed parasites, as previously described (Smirlis *et al.*, 2006, Hombach-Barrigah *et al.*, 2019). More specifically, cells were fixed by addition of ice-cold ethanol and parasitic DNA content was measured by flow cytometry following the incubation with 50 μg mL^{-1} PI and 100 μg mL^{-1} RNase A (Invitrogen) in PBS in

555 the FL2 or 610/20BP channels. For all experiments 10,000 events were collected and analysed.
556 Flow Jo (Miltenyi), MODFIT (Becton-Dickinson) and CELLQuest™ (Becton-Dickinson)
557 software were used to perform the analyses. All flow cytometry experiments were performed at
558 least three times and results presented are from one representative experiment.
559
560 **Fluorescence microscopy**
561 For immunofluorescence analysis, *L. infantum* promastigotes were incubated with 4% (w/v)
562 paraformaldehyde (PF) for 30 min at room temperature (RT). Cells were left to adhere in poly L-
563 lysine coated slides for 20 min. Parasites were blocked with 1% (w/v) BSA in PBS (Sigma
564 Aldrich) and permeabilised with 0.1% (v/v) triton X-100 (Sigma Aldrich) for 30 min and
565 subsequently stained with 1:200 diluted in PBS/ 0,1% (w/v) BSA, mouse anti-alpha tubulin
566 antibody (Sigma, 051M4771) followed by 1 μg mL^{-1} anti-mouse IgG antibody conjugated with
567 Alexa Fluor® 594. Prior to mounting parasites were stained with 2 μM Hoechst 33342 for 15
568 min. Slides were mounted in Vectashield (Vector Laboratories).
569 Analysis of the localisation of *Lin*DYRK1 fusions with eGFP, was performed with
570 staining of live cells with ConA-Alexa594 (Molecular Probes), MitoTracker® Orange
571 CMTMRos (Thermo Fisher Scientific) and FM®4-64FX (Molecular Probes), aided with DNA
572 co-staining with 16 μM Hoechst 33342 (Molecular Probes) according to the manufacturer's
573 instructions. In brief, promastigotes were incubated with 5 μg mL^{-1} of ConA and 20 μg mL^{-1}
574 FM4-64 for 3 min on ice followed by incubation at RT at various time points , and with 100 nM
575 mitotracker for 30 min at RT. ConA stained promastigotes were subjected to live imaging while
576 MitoTracker Orange and FM4-64 stained cells were fixed with 4% (w/v) PF and mounted, as
577 previously reported.
578 Images were collected using the ApoTome inverted (ZEISS) and the confocal
579 microscopes FluoView 1000 (Olympus; Tokyo, Japan) and TCS SP8P (Leica Microsystems

GmbH, Germany). For analysing the morphology of the parasites, images were collected and analysed in Image J software.

Transmission and scanning electron microscopy

Parasites in stationary growth phase were fixed in a solution of 2.5% (v/v) glutaraldehyde, 2 % (v/v) formaldehyde and 2.5 mM $CaCl_2$ in 0.1 M sodium cacodylate buffer pH 7.2, followed by post-fixation in 1% osmium tetroxide and 0.8 % potassium ferrocyanide in the same buffer and acetone gradient dehydration. Finally, the material was embedded in Poly/Bed resin; ultrathin sections were stained with uranyl acetate and lead citrate and observed under a JEM 1320 transmission electron microscope (JEOL). For scanning electron microscopy, parasites were fixed as abovementioned and washed in 0.1 M cacodylate buffer. Cells were left to adhere in poly L-lysine coated slides for 20 min, and post-fixed with a solution of osmium tetroxide containing 0.8–1% of potassium ferrocyanide for 30 min and dehydrated with increasing concentrations of ethanol (30%, 50%, 70%, 90% and 100% (v/v). Samples were subjected to the critical point, metalised with gold and analysed in a JEOL JSM-6390LV scanning electron microscope.

Lectin-mediated agglutination and complement lysis

Agglutination assays using PNA (100 μg μL^{-1}; Sigma) were performed as previously described (Sacks *et al.*, 1985). Stationary phase (day 2 stationary phase) were washed 2 times in PBS and incubated at a density of $3*10^8$ mL^{-1} with PNA in PBS at RT for 30 min and the suspension was centrifuged at 150 x g for 5 min.

Complement lysis of promastigotes was performed according Späth et al., 2003 (Späth *et al.*, 2003). Promastigotes (10^6), were washed and incubated for 30 minutes in 10% (v/v) human serum, that previously separated by centrifugation at 6,000 x g from clotted donor blood, and 50

μg mL^{-1} propidium iodide (Sigma). The percentage of fluorescence (lysis) was determined by flow cytometry.

cDNA synthesis and real-time quantitative reverse transcription-PCR

First strand cDNA was synthesised from 1 μg total RNA using the (Protoscript M-MuLV Taq RT-PCR kit, New England Biolabs) with oligo(dT)18 primers following the manufacturer's instructions. The resulting cDNA was diluted 5 times (10 ng mL^{-1}) with nuclease-free water (NEB). 50 ng of cDNA template were used in a final volume of 20 μL 1X SYBR Green (Kappa Biosystems) based quantitative PCR reactions on a SaCycler-96 RUO cycler (Sacace Biotechnologies, Italy). The protocol used for the qPCR was: 10 s at 94°C, 40 cycles comprising of 30 s at 94°C, 20 s at 52°C, 30 s at 72°C, and a final step of 10 min at 4°C. Primer pairs p15-p16, p17-p18 and p19-p20 were used to amplify meta 1 transcript (*Lin*J.17.0990), HASPB (*Lin*J.23.1220) and prohibitin (*Lin*J.16.1710) respectively (**S4 Table**). The sequences of primer pairs for ribosomal protein S29 transcript (*Lin*J.28.2360) have been previously described (Alexandratos *et al.*, 2013). Gene expression levels were calculated using the comparative C_t method as previously described (Alexandratos *et al.*, 2013), from duplicate or triplicate PCRs of cDNAs synthesised from RNAs recovered from parasites in three different experiments.

Infection of mice and determination of parasite burden with quantitative real-time polymerase chain reaction (qPCR)

Male BALB/c mice (6–8 weeks old) used in the present study were obtained from the breeding unit of the Hellenic Pasteur Institute (HPI; Athens, Greece) and reared in institutional facilities under specific pathogen-free environmental conditions at an ambient temperature of 25°C. Mice were provided with sterile food and water ad libitum. Stationary-phase promastigotes were harvested by centrifugation at 800× g for 10 min at 4°C. The pellet was washed by PBS and

629 resuspended at a concentration of 4×10^8 cells mL-1. A volume of 100 µL of this preparation was
630 injected intravenously in the lateral tail vein of each mouse. Two weeks post infection, mice were
631 sacrificed by CO_2 asphyxiation and 2 mg of liver tissues were frozen for subsequent analysis.
632 DNA was extracted from about 2 mg of liver tissue from infected mice using NucleoSpin® DNA
633 Rapid Lyse (Macherey-Nagel) according to the manufacturer's instructions. Parasite burden was
634 determined using TaqMan-based qPCR assay as previously described (Margaroni *et al.*, 2017,
635 Tellevik *et al.*, 2014). Briefly, the assay was performed in the presence of 15 pmol of forward (5′-
636 7GGCGGCGGTATTATCTCGAT-3′) and 5 pmol of reverse (5′-
637 ACCACGAGGTAGATGACAGACA-3′) primers (VBC Biotech, Vienna, Austria) (targeting a
638 74- bp region of the gene encoding the arginine transporter AAP3 gene) and 25 pmol of TET-
639 labeled TaqMan® probe (TET-5′-ATGTCGGGCATCATC-3′-BHQ; VBC Biotech) and DNA
640 template (50 ng and 100 ng) in a TaqMan master mix (2×) (Kapa Biosystems, Wilmington, MA,
641 USA). Each qPCR test was run in triplicate on a SaCycler-96 RUO cycler (Sacace
642 Biotechnologies, Como, Italy). The cycling conditions were 95°C for 10 min, followed by 40
643 cycles at 95°C, 15 s and 62°C, 60 s. The standard curve method for absolute quantification of
644 parasite number was used. Quantification was performed using standard curves prepared from
645 DNA extracted from ten-fold serial dilution of *L. infantum* parasites (range $1–1\times10^5$).
646
647 **Macrophage infection**
648 Peritoneal macrophages exudate from 6- to 8-week-old female BALB/c mice were collected after
649 4 days injection of 3% (v/v) thioglycollate (Sigma Aldrich), as described previously (Gomes *et*
650 *al.*, 2003). Macrophages were obtained by flushing the peritoneal cavity once with 10 mL ice-
651 cold saline and centrifuged at 300 × g for 10 min. Cells were resuspended in complete RPMI
652 medium, seeded at $2*10^5$/well in 24 well plates containing 13mm-rounded glass slides, and
653 incubated at 37°C, 5% CO_2 overnight. Stationary phase *L. infantum* parasites were plated at a
654 parasite:host cell ratio of 10:1 and incubated for 24 h (time zero) at 37° C 5% CO_2. Infected

cultures were washed extensively with PBS and incubated at the same conditions during 24, 48 and 72 h. Cultures were then fixed with 4% (w/v) paraformaldehyde. DNA was marked with 3 μM DAPI (Sigma Aldrich). Plates were incubated at RT for 10 min followed by wash with PBS. *In vitro* macrophage infections were performed in triplicates in at least three independent experiments. One hundred macrophages were counted per replicate.

Lipid extraction and analysis

Total lipids were extracted from *L. infantum* by the Bligh and Dyer method (Bligh & Dyer, 1959). Briefly, cells in stationary phase were collected by centrifugation (800×g, 10 min), washed with PBS, resuspended in 100 μL PBS and transferred to a glass tube. Following the addition of 375 μL of 1:2 (v/v) $CHCl_3$: MeOH the samples were vortexed thoroughly before further vigorous agitation for 1 hour at 4°C. Biphasic mixtures were generated by the addition of 125 μL of $CHCl_3$ with vortexing and then 125 μL of H_2O again with vortexing followed by centrifugation at 1000×g at RT for 5 min. The lower chloroform-rich phase was transferred to a new glass vial, dried under nitrogen and stored at 4°C. The lipid extracts were dissolved in 50 μL choloroform:methanol (1:2), 50 μL of acetonitrile:isopropanol:water (6:7:2) and 10 mM ammonium acetate and analysed with a Sciex 4000 QTrap, a triple quadrupole mass spectrometer equipped with an AdvionTriVersaNanoMate® source. The nanoelectrospray interface allowed the delivery of samples by direct infusion (~125 nL min^{-1}) with lipids analysed in both positive and negative ion modes using a capillary voltage of 1.25 kV with each spectrum encompassing at least 50 repetitive scans. Tandem mass spectra (MS/MS) were obtained for precursors of phosphatidylinositol (PI)/inositol-phosphoceramide (IPC) species in negative ion mode, with parent-ion scanning of m/z 241 (collision energy of 70V); and phosphatidylcholine (PC)/ sphingomyelin (SM) species in positive mode, with parent-ion scanning of m/z 184 (collision energy of 50V). Assignment of phospholipid species is based upon a combination of survey, daughter and precursor scans, as well as previous assignments (Fernandez-Prada *et al.*, 2016,

Richmond *et al.*, 2010) and use of the LIPID MAPS: Nature Lipidomics Gateway (www.lipidmaps.org).

Identification and characterisation of fatty acids

Total fatty acids were isolated from the *L. infantum* lipid extracts and converted to fatty acid methyl esters (FAME) for GC-MS characterisation following the method of Ichihara and Fukubayashi (2010) (Ichihara & Fukubayashi, 2010). This trans-methylation reaction forms methyl esters of all fatty acids in the sample, regardless of the lipid they were attached to. Briefly, lipid samples were resuspended in 300 µL of 8% (w/v) solution of HCl in methanol water (85:15 v/v) and 200 µL of toluene and 1.5 mL of methanol were added prior to incubation overnight at 45°C. Samples were dried down under nitrogen and 500 µl hexane and 500 µl distilled water were added to create a biphasic mixture, of which the FAME containing upper hexane layer is extracted and dried again under nitrogen. FAME samples were dissolved in 20 µL dichloromethane and analysed by injection of 1 µL into a Agilent Technologies GC-MS (GC-6890N, MS detector-5973) using a ZB-5 column (30 Mx 25 mm x 25mm, Phenomenex) with a temperature program of 50°C for 10 min followed by a rising gradient to 220°C at 5°C /min and hold at 220°C for a further 15 min. Mass spectra were continuously acquired in the range of 50-500 amu and peak identification was performed by comparison of the retention times and fragmentation patterns with a bacterial FAME standard mixture that contains a cyclopropyl C19Δ FAME, in addition to common fatty acids (SIGMA Supelco 47080-U).

Identification and characterisation of sterols

L. infantum lipid extracts were resuspended in 100 µL dichloromethane with 1 µL analysed by gas chromatography-mass spectrometry (GC-MS) on an Agilent Technologies mass selective detector (GC-6890N, MS detector-5973) with a ZB-50 column (15 M x 32 mm ID x 0.5 mm

thickness, (Phenomenex), injector at 270°C with a temperature program of 100°C for 1 min followed by a rising gradient to 200°C at 8°C /min and hold at 200°C for a further 2 min, followed by a second gradient at 3°C /min up to 300°C for a further 15 min. Electron ionisation (EI) was at 70 eV energy, with an emission current of 50 μA and an ion source of 230°C. Mass spectra were acquired from 50-550 amu. Identification was carried out by comparison of the retention times and fragmentation patterns with sterols in the NIST/EPA/NIH Mass Spectral Library and those reported in previous publications (Cauchetier *et al.*, 2002, Fernandez-Prada *et al.*, 2016, Yao & Wilson, 2016). To examine changes in composition, the area under each sterol peak was used for relative quantification.

Ethics statement

All animal protocols were conducted in strict accordance with the National Law 56/2013, which adheres to the European Directive 2010/63/EU for animal experiments, and complied with the Animal Research: Reporting of *In Vivo* Experiments (ARRIVE) guidelines. The study was carried out according to the approved by the Ministry of Rural Development and Food license no. 433-01-2018. The human blood donor sampled was an author of this project. The Bioethics Committee of Hellenic Pasteur Institute was aware of experiments that required human blood in this project, and a waiver was received prior to the initiation of experiments (no.3156).

Acknowledgments

The authors would like to thank Prof. Stephen Beverley for the [pXNG4], [pXGGFP+2], [pXG-PAC] and [pX63-HYG] plasmids and Laura Piel for designing and donating primers p15-p20. The authors would like to thank the Flow Cytometry and Microscopy Units of Hellenic Pasteur Institute and Dr Evangelia Xingi for the help provided, in microscopy analysis. This work was supported by the International Division of the Institute Pasteur (ACIP A13-2013 project), the

Action “KRIPIS I” (MIS 450598) co-financed by European Union and the National Ministry of Education and Religion Affairs under the Operational Strategic Reference Framework (NSRF 2007-2013) and the General Secretariat of Research and Technology (GSRT) and FAPESB/CAPES grant # PET0042/2013 from the Brazilian State and Federal governments, respectively.

Conflict of Interest

None of the authors of the above manuscript has declared any conflict of interest.

Author contributions

VPCR, MD, SYAM, GFS, MBPS and DS have made major contributions to the conception or design of the study, VPCR,MD, SYAM, FK, AE, GFS, MBP and DS to the acquisition, analysis, or interpretation of the data; VPCR GFS, SYA, MBPS and DS to the writing of the manuscript.

References

Alexandratos, A., J. Clos, M. Samiotaki, A. Efstathiou, G. Panayotou, K. Soteriadou & D. Smirlis, (2013) The loss of virulence of histone H1 overexpressing Leishmania donovani parasites is directly associated with a reduction of HSP83 rate of translation. *Mol Microbiol* **88**: 1015-1031.

Almeida, R., B.J. Gilmartin, S.H. McCann, A. Norrish, A.C. Ivens, D. Lawson, M.P. Levick, D.F. Smith, S.D. Dyall, D. Vetrie, T.C. Freeman, R.M. Coulson, I. Sampaio, H. Schneider & J.M. Blackwell, (2004) Expression profiling of the Leishmania life cycle: cDNA arrays identify developmentally regulated genes present but not annotated in the genome. *Mol Biochem Parasitol* **136**: 87-100.

Alvar, J., I.D. Velez, C. Bern, M. Herrero, P. Desjeux, J. Cano, J. Jannin, M. den Boer & W.H.O.L.C. Team, (2012) Leishmaniasis worldwide and global estimates of its incidence. *PLoS One* **7**: e35671.

Aragon, A.D., A.L. Rodriguez, O. Meirelles, S. Roy, G.S. Davidson, P.H. Tapia, C. Allen, R. Joe, D. Benn & M. Werner-Washburne, (2008) Characterization of differentiated quiescent and nonquiescent cells in yeast stationary-phase cultures. *Mol Biol Cell* **19**: 1271-1280.

Aranda, S., A. Laguna & S. de la Luna, (2011) DYRK family of protein kinases: evolutionary relationships, biochemical properties, and functional roles. *FASEB J* **25**: 449-462.

Arisawa, K., H. Mitsudome, K. Yoshida, S. Sugimoto, T. Ishikawa, Y. Fujiwara & I. Ichi, (2016) Saturated fatty acid in the phospholipid monolayer contributes to the formation of large lipid droplets. *Biochem Biophys Res Commun* **480**: 641-647.

Azzopardi, M., G. Farrugia & R. Balzan, (2017) Cell-cycle involvement in autophagy and apoptosis in yeast. *Mechanisms of ageing and development* **161**: 211-224.

Bachmaier, S., R. Witztum, P. Tsigankov, R. Koren, M. Boshart & D. Zilberstein, (2016) Protein kinase A signaling during bidirectional axenic differentiation in *Leishmania*. *Int J Parasitol* **46**: 75-82.

Bates, P.A., (1994) The developmental biology of *Leishmania* promastigotes. *Exp Parasitol* **79**: 215-218.

Becker, W., (2018) A wake-up call to quiescent cancer cells - potential use of DYRK1B inhibitors in cancer therapy. *The FEBS journal* **285**: 1203-1211.

Becker, W. & H.G. Joost, (1999) Structural and functional characteristics of Dyrk, a novel subfamily of protein kinases with dual specificity. *Prog Nucleic Acid Res Mol Biol* **62**: 1-17.

Besteiro, S., R.A. Williams, L.S. Morrison, G.H. Coombs & J.C. Mottram, (2006) Endosome sorting and autophagy are essential for differentiation and virulence of *Leishmania* major. *J Biol Chem* **281**: 11384-11396.

781 Beverley, S.M. & C.E. Clayton, (1993) Transfection of *Leishmania* and *Trypanosoma brucei* by
782 electroporation. *Methods Mol Biol* **21**: 333-348.
783 Bligh, E.G. & W.J. Dyer, (1959) A rapid method of total lipid extraction and purification. *Can J*
784 *Biochem Physiol* **37**: 911-917.
785 Burchmore, R.J. & M.P. Barrett, (2001) Life in vacuoles--nutrient acquisition by *Leishmania*
786 amastigotes. *Int J Parasitol* **31**: 1311-1320.
787 Cauchetier, E., P.M. Loiseau, J. Lehman, D. Rivollet, J. Fleury, A. Astier, M. Deniau & M. Paul,
788 (2002) Characterisation of atovaquone resistance in *Leishmania infantum* promastigotes.
789 *Int J Parasitol* **32**: 1043-1051.
790 Charron, A.J. & L.D. Sibley, (2002) Host cells: mobilizable lipid resources for the intracellular
791 parasite *Toxoplasma gondii*. *J Cell Sci* **115**: 3049-3059.
792 Cunningham, M.L., R.G. Titus, S.J. Turco & S.M. Beverley, (2001) Regulation of differentiation
793 to the infective stage of the protozoan parasite Leishmania major by tetrahydrobiopterin.
794 *Science* **292**: 285-287.
795 da Silva, R. & D.L. Sacks, (1987) Metacyclogenesis is a major determinant of *Leishmania*
796 promastigote virulence and attenuation. *Infect Immun* **55**: 2802-2806.
797 Dacher, M., M.A. Morales, P. Pescher, O. Leclercq, N. Rachidi, E. Prina, M. Cayla, A.
798 Descoteaux & G.F. Späth, (2014) Probing druggability and biological function of
799 essential proteins in *Leishmania* combining facilitated null mutant and plasmid shuffle
800 analyses. *Mol Microbiol* **93**: 146-166.
801 Fernandez-Cortes, F., T.D. Serafim, J.M. Wilkes, N.G. Jones, R. Ritchie, R. McCulloch & J.C.
802 Mottram, (2017) RNAi screening identifies *Trypanosoma brucei* stress response protein
803 kinases required for survival in the mouse. *Sci Rep* **7**: 6156.
804 Fernandez-Prada, C., I.M. Vincent, M.C. Brotherton, M. Roberts, G. Roy, L. Rivas, P. Leprohon,
805 T.K. Smith & M. Ouellette, (2016) Different Mutations in a P-type ATPase Transporter

in *Leishmania* Parasites are Associated with Cross-resistance to Two Leading Drugs by Distinct Mechanisms. *PLoS Negl Trop Dis* **10**: e0005171.

Franke, E.D., P.B. McGreevy, S.P. Katz & D.L. Sacks, (1985) Growth cycle-dependent generation of complement-resistant *Leishmania* promastigotes. *J Immunol* **134**: 2713-2718.

Garrett, S. & J. Broach, (1989) Loss of Ras activity in *Saccharomyces cerevisiae* is suppressed by disruptions of a new kinase gene, YAKI, whose product may act downstream of the cAMP-dependent protein kinase. *Genes Dev* **3**: 1336-1348.

Gomes, I.N., A.F. Calabrich, S. Tavares Rda, J. Wietzerbin, L.A. de Freitas & P.S. Veras, (2003) Differential properties of CBA/J mononuclear phagocytes recovered from an inflammatory site and probed with two different species of *Leishmania*. *Microbes Infect* **5**: 251-260.

Gossage, S.M., M.E. Rogers & P.A. Bates, (2003) Two separate growth phases during the development of *Leishmania* in sand flies: implications for understanding the life cycle. *Int J Parasitol* **33**: 1027-1034.

Hanks, S.K. & T. Hunter, (1995) Protein kinases 6. The eukaryotic protein kinase superfamily: kinase (catalytic) domain structure and classification. *FASEB J* **9**: 576-596.

Hartley, A.D., M.P. Ward & S. Garrett, (1994) The Yak1 protein kinase of *Saccharomyces cerevisiae* moderates thermotolerance and inhibits growth by an Sch9 protein kinase-independent mechanism. *Genetics* **136**: 465-474.

Hombach-Barrigah, A., K. Bartsch, D. Smirlis, H. Rosenqvist, A. MacDonald, F. Dingli, D. Loew, G.F. Späth, N. Rachidi, M. Wiese & J. Clos, (2019) *Leishmania donovani* 90 kD Heat Shock Protein - Impact of Phosphosites on Parasite Fitness, Infectivity and Casein Kinase Affinity. *Sci Rep* **9**: 5074.

Huang, Y., T. Deng & B.W. Winston, (2000) Characterization of hPRP4 kinase activation: potential role in signaling. *Biochem Biophys Res Commun* **271**: 456-463.

Ichihara, K. & Y. Fukubayashi, (2010) Preparation of fatty acid methyl esters for gas-liquid chromatography. *J Lipid Res* **51**: 635-640.

Ilgoutz, S.C., K.A. Mullin, B.R. Southwell & M.J. McConville, (1999) Glycosylphosphatidylinositol biosynthetic enzymes are localized to a stable tubular subcompartment of the endoplasmic reticulum in *Leishmania mexicana*. *EMBO J* **18**: 3643-3654.

Inbar, E., V.K. Hughitt, L.A. Dillon, K. Ghosh, N.M. El-Sayed & D.L. Sacks, (2017) The Transcriptome of *Leishmania major* Developmental Stages in Their Natural Sand Fly Vector. *MBio* **8**.

Jacobs, G., H. Herrmann & G. Gercken, (1982) Incorporation of [1-14C]acetate into fatty acids and aliphatic moieties of glycerolipids in *Leishmania donovani* promastigotes. *Comparative biochemistry and physiology. B, Comparative biochemistry* **73**: 367-373.

Kannan, N. & A.F. Neuwald, (2004) Evolutionary constraints associated with functional specificity of the CMGC protein kinases MAPK, CDK, GSK, SRPK, DYRK, and CK2alpha. *Protein Sci* **13**: 2059-2077.

Kapler, G.M., C.M. Coburn & S.M. Beverley, (1990) Stable transfection of the human parasite Leishmania major delineates a 30-kilobase region sufficient for extrachromosomal replication and expression. *Mol Cell Biol* **10**: 1084-1094.

Laemmli, U.K., (1970) Cleavage of structural proteins during the assembly of the head of bacteriophage T4. *Nature* **227**: 680-685.

Lochhead, P.A., G. Sibbet, N. Morrice & V. Cleghon, (2005) Activation-loop autophosphorylation is mediated by a novel transitional intermediate form of DYRKs. *Cell* **121**: 925-936.

Madeira da Silva, L. & S.M. Beverley, (2010) Expansion of the target of rapamycin (TOR) kinase family and function in *Leishmania* shows that TOR3 is required for acidocalcisome biogenesis and animal infectivity. *Proc Natl Acad Sci U S A* **107**: 11965-11970.

858 Margaroni, M., M. Agallou, E. Athanasiou, O. Kammona, C. Kiparissides, C. Gaitanaki & E.
859 Karagouni, (2017) Vaccination with poly(D,L-lactide-co-glycolide) nanoparticles loaded
860 with soluble *Leishmania* antigens and modified with a TNFalpha-mimicking peptide or
861 monophosphoryl lipid A confers protection against experimental visceral leishmaniasis.
862 *Int J Nanomedicine* **12**: 6169-6184.
863 McConville, M.J. & T. Naderer, (2011) Metabolic pathways required for the intracellular survival
864 of *Leishmania*. *Annu Rev Microbiol* **65**: 543-561.
865 Mony, B.M., P. MacGregor, A. Ivens, F. Rojas, A. Cowton, J. Young, D. Horn & K. Matthews,
866 (2014) Genome-wide dissection of the quorum sensing signalling pathway in
867 *Trypanosoma brucei*. *Nature* **505**: 681-685.
868 Murakami, N., D. Bolton & Y.W. Hwang, (2009) Dyrk1A binds to multiple endocytic proteins
869 required for formation of clathrin-coated vesicles. *Biochemistry* **48**: 9297-9305.
870 Murakami, N., D.C. Bolton, E. Kida, W. Xie & Y.W. Hwang, (2012) Phosphorylation by Dyrk1A
871 of clathrin coated vesicle-associated proteins: identification of the substrate proteins and
872 the effects of phosphorylation. *PLoS One* **7**: e34845.
873 Murray, H.W., J.D. Berman, C.R. Davies & N.G. Saravia, (2005) Advances in leishmaniasis.
874 *Lancet* **366**: 1561-1577.
875 Murta, S.M., T.J. Vickers, D.A. Scott & S.M. Beverley, (2009) Methylene tetrahydrofolate
876 dehydrogenase/cyclohydrolase and the synthesis of 10-CHO-THF are essential in
877 *Leishmania major*. *Mol Microbiol* **71**: 1386-1401.
878 Nourbakhsh, F., S.R. Uliana & D.F. Smith, (1996) Characterisation and expression of a stage-
879 regulated gene of *Leishmania major*. *Mol Biochem Parasitol* **76**: 201-213.
880 Papageorgiou, F.T. & K.P. Soteriadou, (2002) Expression of a novel Leishmania gene encoding a
881 histone H1-like protein in *Leishmania major* modulates parasite infectivity in vitro. *Infect*
882 *Immun* **70**: 6976-6986.

Parsons, M., E.A. Worthey, P.N. Ward & J.C. Mottram, (2005) Comparative analysis of the kinomes of three pathogenic trypanosomatids: *Leishmania major*, *Trypanosoma brucei* and *Trypanosoma cruzi*. *BMC Genomics* **6**: 127.

Petan, T., E. Jarc & M. Jusovic, (2018) Lipid Droplets in Cancer: Guardians of Fat in a Stressful World. *Molecules* **23**.

Pletnev, P., I. Osterman, P. Sergiev, A. Bogdanov & O. Dontsova, (2015) Survival guide: *Escherichia coli* in the stationary phase. *Acta naturae* **7**: 22-33.

Richmond, G.S., F. Gibellini, S.A. Young, L. Major, H. Denton, A. Lilley & T.K. Smith, (2010) Lipidomic analysis of bloodstream and procyclic form *Trypanosoma brucei*. *Parasitology* **137**: 1357-1392.

Sacks, D.L., S. Hieny & A. Sher, (1985) Identification of cell surface carbohydrate and antigenic changes between noninfective and infective developmental stages of *Leishmania major* promastigotes. *J Immunol* **135**: 564-569.

Sacks, D.L. & P.V. Perkins, (1984) Identification of an infective stage of *Leishmania promastigotes*. *Science* **223**: 1417-1419.

Sacks, D.L. & P.V. Perkins, (1985) Development of infective stage *Leishmania* promastigotes within phlebotomine sand flies. *Am J Trop Med Hyg* **34**: 456-459.

Sadlova, J., H.P. Price, B.A. Smith, J. Votypka, P. Volf & D.F. Smith, (2010) The stage-regulated HASPB and SHERP proteins are essential for differentiation of the protozoan parasite *Leishmania major* in its sand fly vector, Phlebotomus papatasi. *Cell Microbiol* **12**: 1765-1779.

Schmitz, M.L., A. Rodriguez-Gil & J. Hornung, (2014) Integration of stress signals by homeodomain interacting protein kinases. *Biol Chem* **395**: 375-386.

Serafim, T.D., A.B. Figueiredo, P.A. Costa, E.A. Marques-da-Silva, R. Goncalves, S.A. de Moura, N.F. Gontijo, S.M. da Silva, M.S. Michalick, J.R. Meyer-Fernandes, R.P. de

908 Carvalho, S.R. Uliana, J.L. Fietto & L.C. Afonso, (2012) *Leishmania* metacyclogenesis is
909 promoted in the absence of purines. *PLoS Negl Trop Dis* **6**: e1833.
910 Silva, A.M., A. Cordeiro-da-Silva & G.H. Coombs, (2011) Metabolic variation during
911 development in culture of Leishmania donovani promastigotes. *PLoS Negl Trop Dis* **5**:
912 e1451.
913 Smirlis, D., S.N. Bisti, E. Xingi, G. Konidou, M. Thiakaki & K.P. Soteriadou, (2006) *Leishmania*
914 histone H1 overexpression delays parasite cell-cycle progression, parasite differentiation
915 and reduces Leishmania infectivity in vivo. *Mol Microbiol* **60**: 1457-1473.
916 Smirlis, D., M. Duszenko, A.J. Ruiz, E. Scoulica, P. Bastien, N. Fasel & K. Soteriadou, (2010)
917 Targeting essential pathways in trypanosomatids gives insights into protozoan
918 mechanisms of cell death. *Parasit Vectors* **3**: 107.
919 Soppa, U. & W. Becker, (2015) DYRK protein kinases. *Curr Biol* **25**: R488-489.
920 Späth, G.F., L.A. Garraway, S.J. Turco & S.M. Beverley, (2003) The role(s) of
921 lipophosphoglycan (LPG) in the establishment of *Leishmania major* infections in
922 mammalian hosts. *Proceedings of the National Academy of Sciences of the United States*
923 *of America* **100**: 9536-9541.
924 Stierhof, Y.D., T. Ilg, D.G. Russell, H. Hohenberg & P. Overath, (1994) Characterization of
925 polymer release from the flagellar pocket of *Leishmania mexicana* promastigotes. *J Cell*
926 *Biol* **125**: 321-331.
927 Tanz, S.K., I. Castleden, I.D. Small & A.H. Millar, (2013) Fluorescent protein tagging as a tool to
928 define the subcellular distribution of proteins in plants. *Front Plant Sci* **4**: 214.
929 Tellevik, M.G., K.E. Muller, K.R. Lokken & A.H. Nerland, (2014) Detection of a broad range of
930 *Leishmania* species and determination of parasite load of infected mouse by real-time
931 PCR targeting the arginine permease gene AAP3. *Acta Trop* **137**: 99-104.

Tsigankov, P., P.F. Gherardini, M. Helmer-Citterich, G.F. Späth, P.J. Myler & D. Zilberstein, (2014) Regulation dynamics of *Leishmania* differentiation: deconvoluting signals and identifying phosphorylation trends. *Mol Cell Proteomics* **13**: 1787-1799.

Tsigankov, P., P.F. Gherardini, M. Helmer-Citterich, G.F. Späth & D. Zilberstein, (2013) Phosphoproteomic analysis of differentiating *Leishmania* parasites reveals a unique stage-specific phosphorylation motif. *J Proteome Res* **12**: 3405-3412.

Walther, T.C. & R.V. Farese, Jr., (2012) Lipid droplets and cellular lipid metabolism. *Annual review of biochemistry* **81**: 687-714.

Williams, R.A., L. Tetley, J.C. Mottram & G.H. Coombs, (2006) Cysteine peptidases CPA and CPB are vital for autophagy and differentiation in *Leishmania mexicana*. *Mol Microbiol* **61**: 655-674.

Wozencraft, A.O. & J.M. Blackwell, (1987) Increased infectivity of stationary-phase promastigotes of *Leishmania donovani*: correlation with enhanced C3 binding capacity and CR3-mediated attachment to host macrophages. *Immunology* **60**: 559-563.

Yao, C. & M.E. Wilson, (2016) Dynamics of sterol synthesis during development of *Leishmania* spp. parasites to their virulent form. *Parasit Vectors* **9**: 200.

Tables

Table 1: Fatty acid and sterol content of *Lin*DYRK1$^{-/-}$ promastigotes and control wild type *Lin*DYRK1$^{+/+}$ and parental *Lin*DYRK1$^{-/-}$[pXNG-*Lin*DYRK1] cell lines

		Mean mol % ±SD			
		*Lin*DYRK1$^{+/+}$	*Lin*DYRK1$^{-/-}$ [pXNG-*Lin*DYRK1]**A**	*Lin*DYRK1^{-}$^{/-}$**A1**	*Lin*DYRK1^{-}$^{/-}$**B1**
Fatty acids	14:00	1.70± 0.5	0.51 ± 0.09	0.63± 0.07	0.47± 0.32
	16:01	0.79± 0.56	0.42 ± 0.29	0.63 ± 0.19	1.10± 0.18
	16:00	8.23 ± 1.70	9.37 ± 4.25	11.71± 1.67	9.33± 0.94
	18:02	24.50± 1.70	19.24 ± 5.58	14.98 ± 6.36*	15.73± 0.52*

	18:01	41.57± 2.37	44.12 ± 3.31	41.87± 0.75	42.66± 0.29
	18:00	14.14± 0.73	17.19 ± 3.70	22.05± 3.01**	19.91± 1.68**
	C19Δ	5.46± 0.55	4.24 ±1.12	4.75± 1.12	7.12± 0.51
	20:02	2.64± 0.19	2.62± 0.00	2.09 ± 0.13	2.30± 0.06
	20:00	0.98± 0.21	2.29 ±1.68	1.29 ± 0.20	1.40± 0.09
	SFA	25.0± 3.14	29.4± 9.72	35.7± 4.81	31.1± 0.52
	MUFA	47.8± 1.26	48.8± 4.12	47.2± 1.67	50.9± 0.98
	PUFA	27.1± 1.88	21.9± 5.57	17.1± 6.48	18.0± 0.46
Sterol (retention time min^{-1})	Cholesterol (35.21)	27.66± 2.98	15.27± 0.01	14.49± 2.23	14.97± 4.66
	Zymosterol (33.59)	4.14± 0.75	7.47± 4.97	12.48± 1.28	4.51± 1.45
	Cholesta-5,7,24-trien-3β-ol (30.21)	8.57± 0.08	6.50± 1.46	7.55± 0.2	5.79± 2.37
	Ergosterol (35.21)	30.23± 0.54	29.92± 2.08	31.44± 3.82	30.83± 2.05
	Ergosta-7,24-dien-3β-ol (35.76)	11.71±0	18.66± 3.97	17.84± 0.28	22.18± 1.12
	14α-methylergosta-8,24(28)-dien-3β-ol (36.02)	4.53± 0.31	4.57± 2.22	5.38± 1.59	3.33± 0.09
	14α-methylergosta-5,7,24(28)-trien-3β-ol	6.42± 0.20	3.46± 0.79	3.80± 1.36	3.02± 0.21
	Lanosterol (36.47)	0.00± 0.00	4.99± 7.05	0.00± 0.00	8.93± 0.21
	4,14α-dimethylergosta-8,24(28)-dien-3β-ol (36.75)	2.23±0.70	3.42± 1.97	3.11± 2.94	1.67± 2.36
	Stigmasta-7,24(28)-dien-3β-ol (37.85)	4.51± 2.20	5.74± 1.71	3.91± 0.96	4.77± 1.56

Table 1 legend: Fatty acid and sterol composition was determined by GC analysis as described in Materials and Methods section. Data, expressed as mole percent, are means ±SD of 2 independent experiments. SFA = Saturated fatty acids, MUFA = monounsaturated fatty acids, PUFA = polyunsaturated fatty acids**. ***p< 0.01, two-tail, paired student's t test between the replicates of mutants and the corresponding control values (*Lin*DYRK1$^{+/+}$ and *Lin*DYRK1$^{-/-}$ [pXNG-*Lin*DYRK1;** p=0.057, two-tail, paired Student's t test between the replicates of mutants and the corresponding control values (*Lin*DYRK1$^{+/+}$ and *Lin*DYRK1$^{-/-}$[pXNG-*Lin*DYRK1).

Figure legends

Fig 1. DYRK family in *Leishmania* and sequence comparison of two related *Leishmania* DYRKs: *Lin*DYRK1 (*LinJ*.15.0180) and *LinJ*.14.0890

(A) Representation of unrooted phylogenetic tree of DYRK kinases using as input full protein sequences. DYRK families and sub-families are indicated. The leishmanial DYRKs are highlighted according to DYRK subfamilies colour. *Lin*DYRK1 (*Lin*.15.0180) is in bold red. Accession numbers are shown in **S3 Table.** (B) Sequence comparison of two related *Leishmania* DYRKs: *Lin*DYRK1 (*LinJ*.15.0180) and *LinJ*.14.0890. Conserved identical residues are shaded in black. Different protein sequences or motifs are shown. PEST sequence is shown in violet [predicted by epestfind (http://emboss.bioinformatics.nl/cgi-bin/emboss/epestfind)] and DYRK homology box (DH box) in green. Secondary structure predictions (α helix blue, β sheet orange) of the kinase domains corresponding to the DYRK1A kinase domain (http:// www.rcb.org/pdb/home.home.do). Lines indicate kinase subdomains (I-XI) according to Hanks and Hunter, 1995 (Hanks & Hunter, 1995) and functional features including the ATP anchor, phosphate anchor, catalytic loop, cation binding site, activation loop, P+1 loop and CMGC insert (red line). Grey represents important insertions in the sequence of *LinJ*.14.0890. Red arrow represents the activation loop tyrosine (Y).

Fig 2. Localisation of GFP-*Lin*DYRK1 in *Leishmania* promastigotes (A) Fluorescence confocal microscopy showing the localisation of the GFP-*Lin*DYRK1 hybrid protein (GFP-*Lin*DYRK1, green) in logarithmic (scale bar = 10 μm), early stationary (scale bar = 10μm) and late stationary promastigotes (scale bar upper row= 10 μm; scale bar lower row= 5 μm). Promastigotes were stained with mitotracker (mitotracker, red) to visualise the mitochondrion and Hoechst 33342 (Hoechst, blue) to visualise the nucleus (N) and kinetoplast (K). Bright field and images with merged channels are also shown. (B) Live imaging showing the localisation of GFP-*Lin*DYRK1 (green) *L. amazonensis* logarithmic promastigotes, in cells treated for 3 min with ConA-Alexa594 (ConA, red) and Hoechst (blue) to visualise the nucleus (N) and kinetoplast (K). Scale bar= 5 μM. (C) Fluorescence confocal microscopy showing the localisation of the GFP-*Lin*DYRK1fusion protein (GFP-*Lin*DYRK1, green) in logarithmic cells stained with FM®4-

64FX (FM4-64, Red) (pulse chase experiment) for 20 min at 4^{o}C to visualise the endosomal compartment and Hoechst 33342 (Hoechst, blue) to visualise the nucleus (N) and kinetoplast (K). Bright field and images with merged channels are also shown Scale bar=10 μm, Insets: 2-fold magnification

Fig 3. Growth-curve and cell cycle analysis of *Lin*DYRK1 over-expressing promastigotes

(A) Growth-curve of *Lin*DYRK1 over-expressing parasites. Left panel: 10^6 ml^{-1} starting inoculum. The growth of wild type promastigotes (*Lin*DYRK1$^{+/+}$), of promastigotes transfected with episome only (*Lin*DYRK1$^{+/+}$[pXNG]), of promastigotes transfected with pXNG-*Lin*DYRK1 (*Lin*DYRK1$^{+/+}$[pXNG-*Lin*DYRK1]) and of promastigotes that had lost the episome after 15 passages of negative selection in GCV (*Lin*DYRK1$^{+/+}$[pXNG-*Lin*DYRK1]GCV), seeded at 10^6 mL^{-1} was monitored daily by cell count. Bars indicate the mean ± standard deviation (SD) of five independent experiments. Right panel: 3 *10^5 mL^{-1} starting inoculum. The growth of promastigotes transfected with episome only (*Lin*DYRK1$^{+/+}$[pXNG]), of promastigotes transfected with pXNG-*Lin*DYRK1 (*Lin*DYRK1$^{+/+}$[pXNG-*Lin*DYRK1]). Bars indicate the mean ± standard deviation (SD) of three independent experiments. (B) Cell cycle analysis of *Lin*DYRK1 transgenic parasites showing overlaid histogram plots of *Lin*DYRK1$^{+/+}$[pXNG-*Lin*DYRK1] (light blue) and *Lin*DYRK1$^{+/+}$[pXNG] (pink) promastigotes. Cell cycle analysis was performed in promastigotes synchronised in the G_1/S cell boundary with 2.5 mM HU for 12 h or in promastigotes after 3 h and 6.5 h post-HU release. Diploid (2N) and tetraploid (4N) DNA content is indicated. This experiment is representative of three experiments performed.

Fig 4. Time-course analysis of *Lin*DYRK1$^{-/-}$[pXNG-*Lin*DYRK1] by negative GCV selection

(A) Green fluorescent histograms (FL-1) of *Lin*DYRK1$^{-/-}$[pXNG-*Lin*DYRK1] clones (A and B) during 4 cell culture passages with 50 μg mL^{-1} GCV (GCVp1- GCVp4) are used to quantify GFP levels and hence the presence of [pXNG-*Lin*DYRK1]. GCV treated clones were compared to

clones cultivated with 150 μg mL^{-1} of the positive selection drug, NTC (NTC). *Lin*DYRK1$^{+/+}$ [pXNG-*Lin*DYRK1] parasites were used as control, and wild type cells were used to determine the background fluorescence level. The perpendicular line separates GFP positive fluorescence from the background fluorescence level. (B) Histograms that show the percentage of retained GFP fluorescence for *Lin*DYRK1$^{-/-}$[pXNG-*Lin*DYRK1] clones A and B, of 4 passages of selection with 50 μg mL^{-1} GCV (GCVp1- GCVp4) with respect to the GFP fluorescence of the same cells treated with 150 μg mL-1 NTC (NTC). *Lin*DYRK1$^{+/+}$ [pXNG-*Lin*DYRK1] parasites were used as control. This experiment was performed three times and error bars represent the standard deviation of three different experiments. (C) Western blot analysis after 15 passages of selection with 50 μg mL^{-1} GCV. Twenty μg of total protein was extracted from late logarithmic phase promastigotes, was analysed by immunoblotting with anti-GFP antibody (GFP, and anti-alpha tubulin antibody (alpha tubulin) for normalisation. Left: Total protein extracts were analysed from late logarithmic *Lin*DYRK1$^{+/+}$[pXNG-*Lin*DYRK1] pool maintained in NTC, or after 15 passages of negative selection with GCV or of passive selection (no drug). Right: Total protein extracts from individual clones derived from pools of *Lin*DYRK1$^{-/-}$[pXNG-*Lin*DYRK1] cells (clone B) after 15 passages of negative selection (GCV) and of the same pool cultivated in the presence of NTC as a positive control. Here we only show the western blots derived from heterozygous clone **B**, but similar results were observed for clone **A**.

Fig 5. *Lin*DYRK1$^{-/-}$display aberrant morphology and increased cell-death in stationary growth-phase and during heat-shock

(A) Morphology of *Lin*DYRK1$^{-/-}$ promastigotes in stationary phase. Upper panel and lower left: Morphometric measurements showing roundness, body length and body width of *Lin*DYRK1$^{-/-}$**A1** and **A2** clones, *Lin*DYRK1$^{-/-}$[pXNG-*Lin*DYRK1]A parental clone, *Lin*DYRK1$^{-/-}$ add back (**A1** clone) and *Lin*DYRK1$^{+/+}$ wild type cells. Bars represent mean ± SEM. * Statistically significant ($p < 0.05$). Lower right: Immunofluorescence analysis of stationary phase *Lin*DYRK1$^{-/-}$

promastigotes and add back showing the morphology of alpha tubulin and DNA stained cells. Fluorescence microscopy shows nuclear and kinetoplast DNA, after labelling with Hoechst 33342 (Hoechst, blue), and alpha tubulin (α tubulin, red) after labelling with anti-alpha tubulin antibody and secondary anti-mouse Alexa Fluor® 594 (alpha tubulin, red). Scale bar= 1.5 μm. (B) DNA content determination of *Lin*DYRK1$^{-/-}$ promastigotes in logarithmic and late stationary (day 3) growth phase by flow cytometry. Flow cytometry profiles showing the DNA content of control wild type parasites *Lin*DYRK1$^{+/+}$, parental cell line *Lin*DYRK1$^{-/-}$[pXNG-*Lin*DYRK1]**A** and two independent knockout mutants *Lin*DYRK1$^{-/-}$**A1** and *Lin*DYRK1$^{-/-}$**A2** and the *Lin*DYRK1$^{-/-}$**A1** add back. Diploid (2N) and tetraploid (4N) DNA content is indicated. Arrows indicate great increase of hypodiploid DNA content. This is a representative experiment of three.

Fig 6. Ultrastructural alterations and fatty acid composition in *Lin*DYRK1 null mutants

(A) Scanning electron microscopy (SEM) of *Lin*DYRK1 promastigotes in stationary phase. SEM showing the rounded promastigote cell shape and membrane alterations of stationary phase *Lin*DYRK1$^{-/-}$ null mutants and comparison with wild type *Lin*DYRK1$^{+/+}$ and parental cell line *Lin*DYRK1$^{-/-}$[pXNG-*Lin*DYRK1] in the same growth phase. Arrows indicate sites of surface irregularities and membrane invaginations of null mutants. Scale bars are indicated on each image (B) Transmission electron microscopy (TEM) of *Lin*DYRK1 promastigotes in stationary phase. TEM analysis of (I) wild type *Lin*DYRK1$^{+/+}$, (II) *Lin*DYRK1$^{-/-}$[pXNG-*Lin*DYRK1] and (III-VI) *Lin*DYRK1$^{-/-}$ stationary phase promastigotes. Figure shows increased accumulation of lipid (Ld) bodies in null mutant parasites. Black arrow in V indicates kinetoplast membrane inside a vacuole and white arrows (III, IV) show open membrane invaginations filled with lipids (IV, V). Scale bars are indicated on each image. N, nuclei; K, kinetoplast; Fp, flagellar pocket; V, vacuole. (C) Fatty acid composition of *L. infantum* promastigotes in stationary phase. Composition of total fatty acids isolated from *Lin*DYRK1$^{+/+}$, *Lin*DYRK1$^{+/+}$[pXNG-LinDYRK1] and *Lin*DYRK1$^{-/-}$ mutants. Total fatty acids from two independent cultures of *Lin*DYRK1$^{+/+}$, *Lin*DYRK1$^{+/+}$[pXNG-

*Lin*DYRK1]**A** and two independent clones derived from different parental mutants *Lin*DYRK1$^{-/-}$ **A** and *Lin*DYRK1$^{-/-}$**B** were analysed with gas chromatography mass spectrometry (GC-MS). Bars show the mean values percentages of saturated (0 double bonds), monounsaturated (1 double bond) and polyunsaturated fatty acids (≥2 double bonds).

Fig 7. Reduction of virulent traits, compromised survival in mouse peritoneal macrophages and increased heat shock sensitivity of *Lin*DYRK1$^{-/-}$ promastigotes

(A) Column charts displaying the percentage of lysed (propidium iodide positive, PI+) *Lin*DYRK1$^{+/+}$, *Lin*DYRK1$^{-/-}$[pXNG-*Lin*DYRK1] and *Lin*DYRK1$^{-/-}$ logarithmic (Log) and stationary (Stat) growth phase promastigotes by serum complement. Bars show the mean ± standard error of the mean (SEM) of at least three experiments performed. Statistically significant * ($p < 0.05$) (Student's *t* paired test). (B) Column charts displaying the percentage of live (propidium iodide negative, PI-) unagglutinated *Lin*DYRK1$^{+/+}$, *Lin*DYRK1$^{-/-}$[pXNG-*Lin*DYRK1] and *Lin*DYRK1$^{-/-}$ promastigotes after PNA agglutination assay. Bars show the mean ± standard deviation (SD) of at least three experiments performed. Statistically significant * ($p < 0.01$), ** ($p<0.05$) (Student's *t* paired test). (C) Expression of prohibitin (*Lin*J.16.1710), meta 1 (*Lin*J.17.0990) and HASPB (*Lin*J23.1220) transcripts Meta-1 transcripts, relative to ribosomal protein S29 transcript (*Lin*J.28.2360) in stationary phase *Lin*DYRK1$^{+/+}$, *Lin*DYRK1$^{-/-}$[pXNG-*Lin*DYRK1] and *Lin*DYRK1$^{-/-}$ promastigotes by qPCR assessment. Expression levels are the mean of 3 independent experiments (3 independent cDNAs per cell line). Statistically significant * ($p<0.05$). (D) Cell cycle analysis of *Lin*DYRK1$^{-/-}$ promastigotes under heat-shock. *Lin*DYRK1$^{+/+}$, *Lin*DYRK1$^{-/-}$[pXNG-*Lin*DYRK1], *Lin*DYRK1$^{-/-}$A1 and *Lin*DYRK1$^{-/-}$A2 and *Lin*DYRK1$^{-/-}$ add back (A1 clone) promastigotes in logarithmic growth phase cultivated at 26°C and 37°C for 16 h. Diploid (2N) and tetraploid (4N) DNA content is indicated. Results are representative of 3 experiments. Arrows show the increased percentage of hypodiploid cells. (E) Reduced intracellular survival in peritoneal macrophages of *Lin*DYRK1$^{-/-}$ parasites in comparison

to survival of *Lin*DYRK1$^{-/-}$[pXNG-*Lin*DYRK1] and *Lin*DYRK1$^{+/+}$ promastigotes. The numbers of parasites per cell, as well as the percentage of infection at 0 h and 72 h post-infection were calculated based on the number of parasite and host nuclei. Bars show the mean ± SEM of three experiments performed.

A

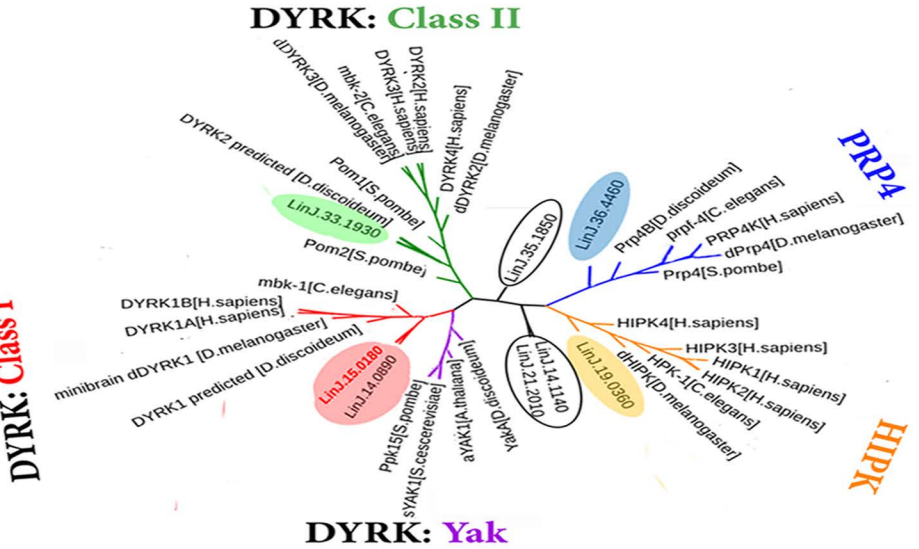
DYRK: Class II
dDYRK3[D.melanogaster]
mbk-2[C.elegans]
DYRK3[H.sapiens]
DYRK2[H.sapiens]
DYRK4[H.sapiens]
dDYRK2[D.melanogaster]
DYRK2 predicted [D.discoideum]
Pom1[S.pombe]
LinJ.33.1930
Pom2[S.pombe]
LinJ.35.1850
LinJ.36.4460
Prp4B[D.discoideum]
prp-4[C.elegans]
PRP4K[H.sapiens]
dPrp4[D.melanogaster]
Prp4[S.pombe]
PRP4
mbk-1[C.elegans]
DYRK1B[H.sapiens]
DYRK1A[H.sapiens]
minibrain dDYRK1 [D.melanogaster]
DYRK1 predicted [D.discoideum]
DYRK: Class I
LinJ.15.0180
LinJ.14.0890
Ppk15[S.pombe]
sYak1[S.cescerevisiae]
aYak1[A.thaliana]
hYak1[H.sapiens]
LinJ.14.1140
LinJ.21.2010
LinJ.19.0360
HIPK4[H.sapiens]
HIPK3[H.sapiens]
HIPK1[H.sapiens]
HIPK2[H.sapiens]
dHIPK[D.melanogaster]
HPK-1[C.elegans]
HIPK
DYRK: Yak

B

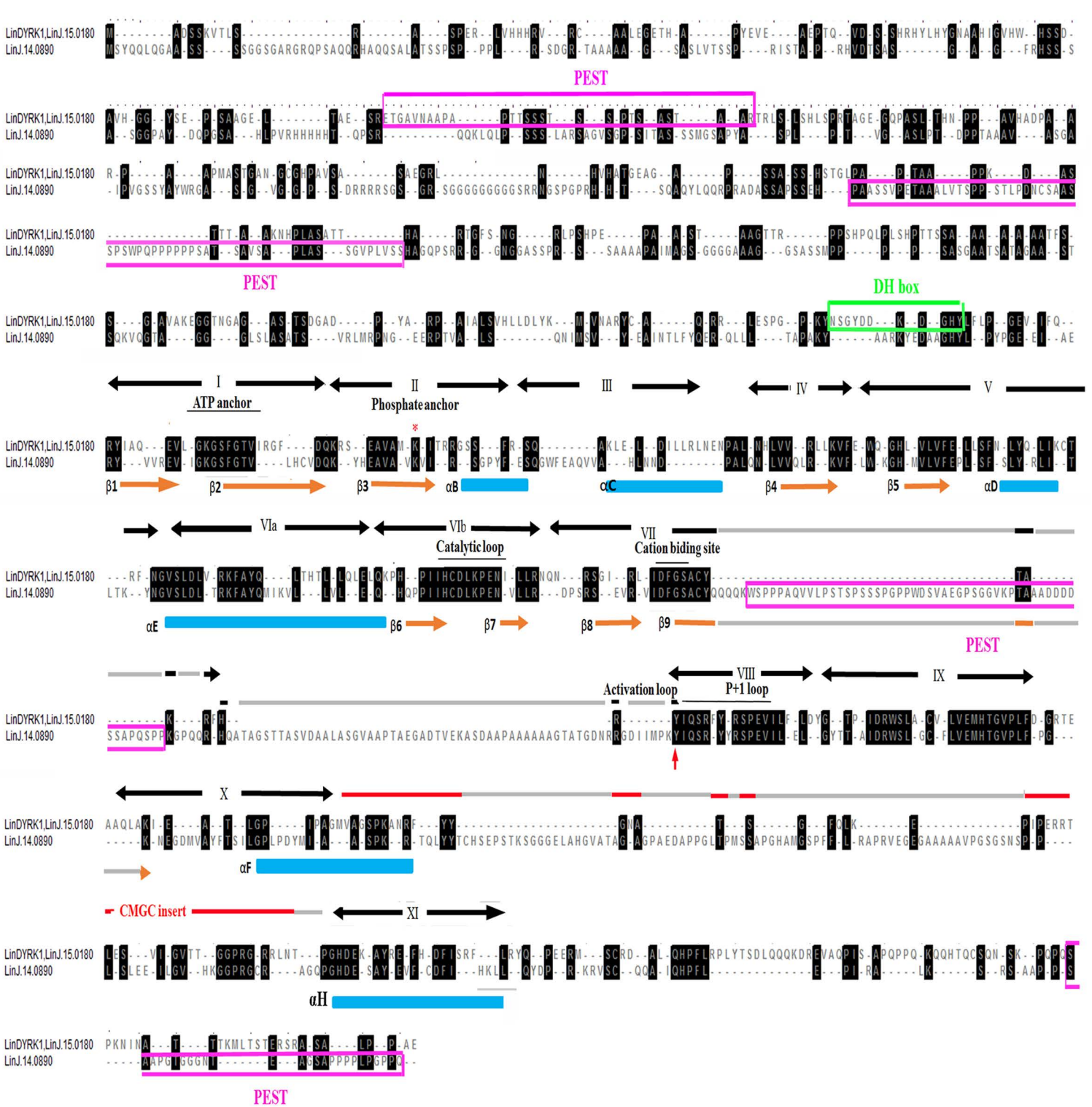
LinDYRK1,LinJ.15.0180
LinJ.14.0890
PEST
ATP anchor
Phosphate anchor
DH box
Catalytic loop
Cation biding site
Activation loop
P+1 loop
CMGC insert

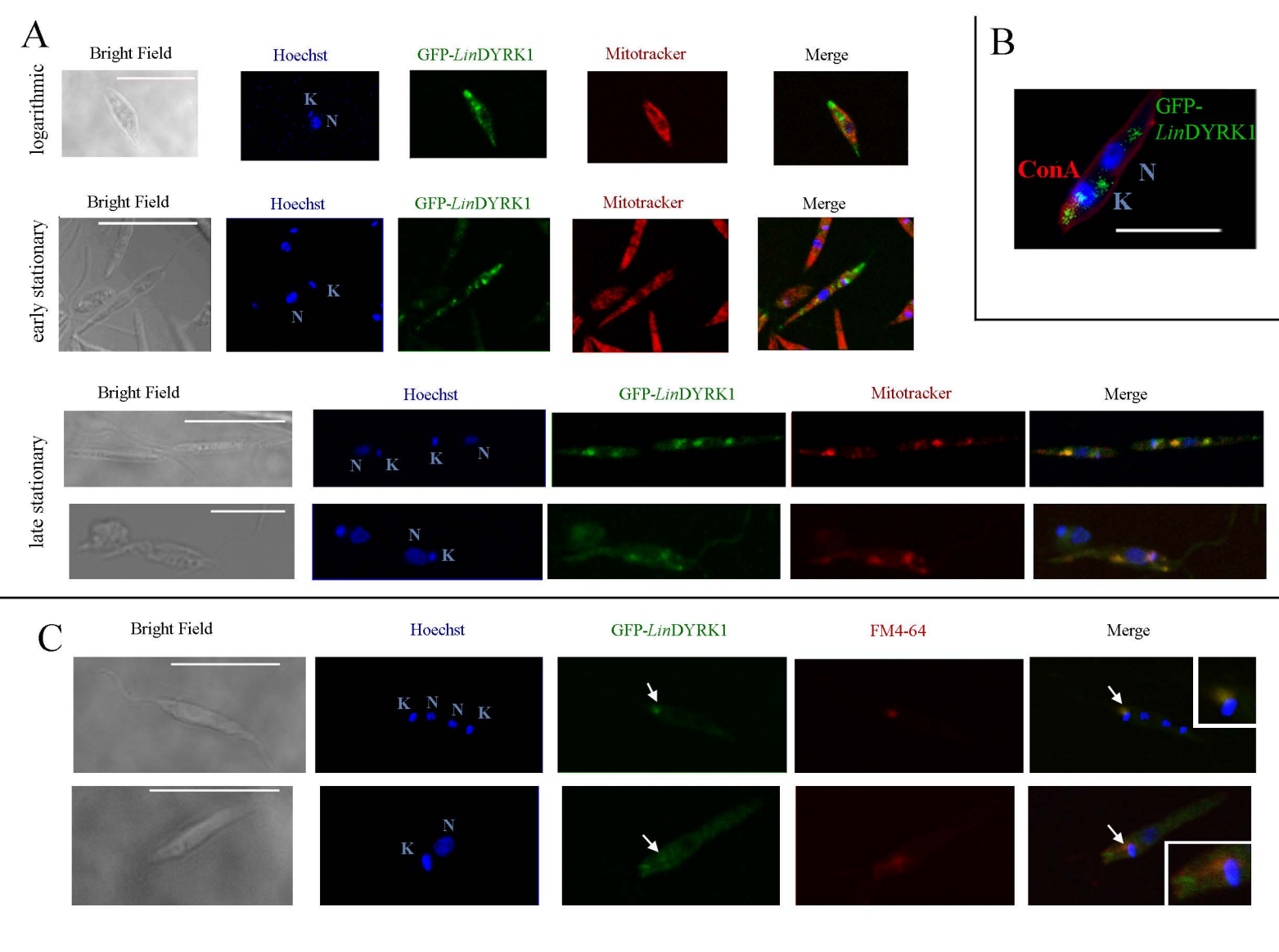
A
Bright Field
Hoechst
GFP-LinDYRK1
Mitotracker
Merge
logarithmic
K
N
early stationary
late stationary
B
ConA
GFP-LinDYRK1
N
K
C
FM4-64

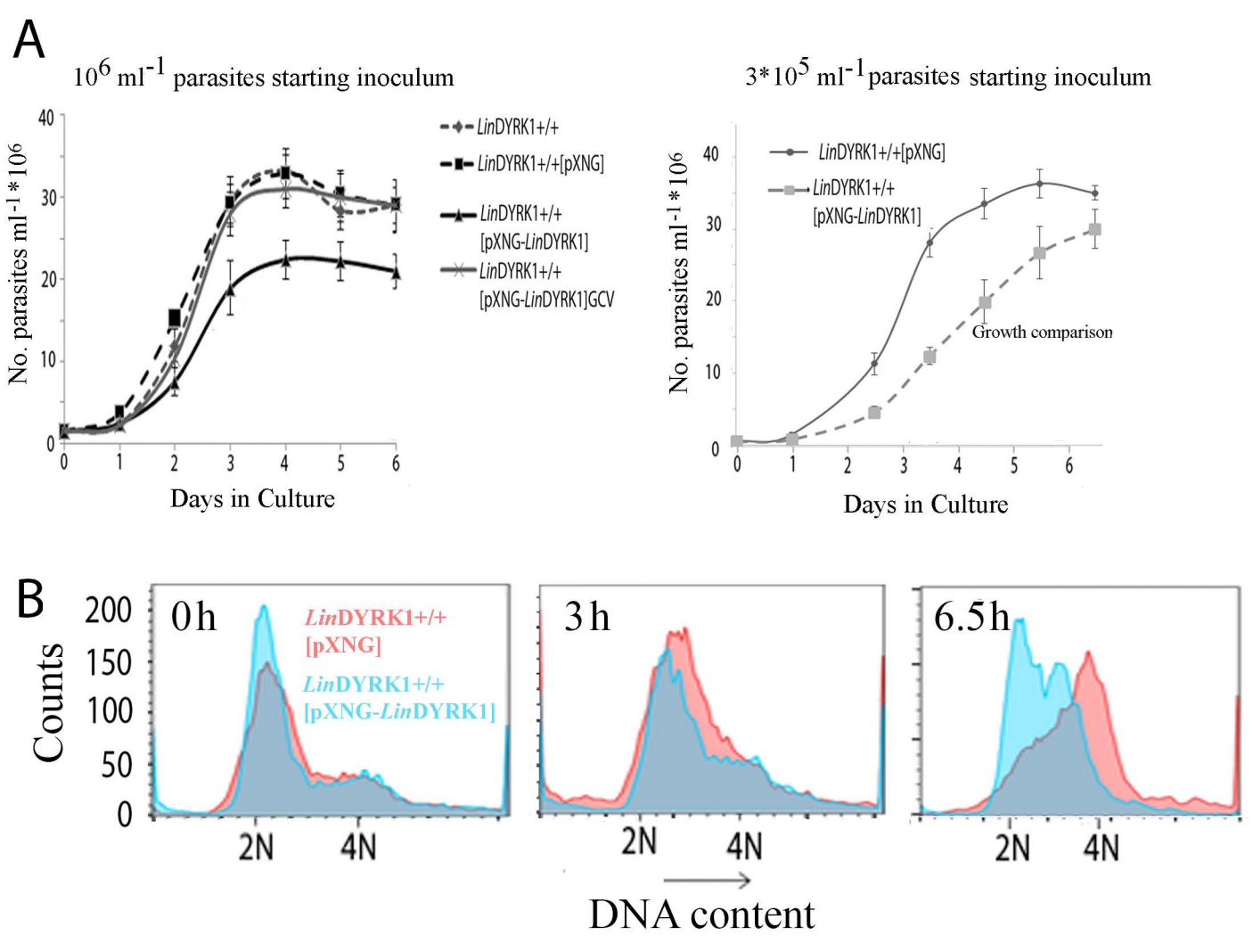
A
10^6 ml^-1 parasites starting inoculum
No. parasites ml^-1 *10^6
Days in Culture
LinDYRK1+/+
LinDYRK1+/+[pXNG]
LinDYRK1+/+ [pXNG-LinDYRK1]
LinDYRK1+/+ [pXNG-LinDYRK1]GCV
3*10^5 ml^-1 parasites starting inoculum
LinDYRK1+/+[pXNG]
LinDYRK1+/+ [pXNG-LinDYRK1]
Growth comparison
B
Counts
0h
3h
6.5h
LinDYRK1+/+ [pXNG]
LinDYRK1+/+ [pXNG-LinDYRK1]
2N
4N
DNA content

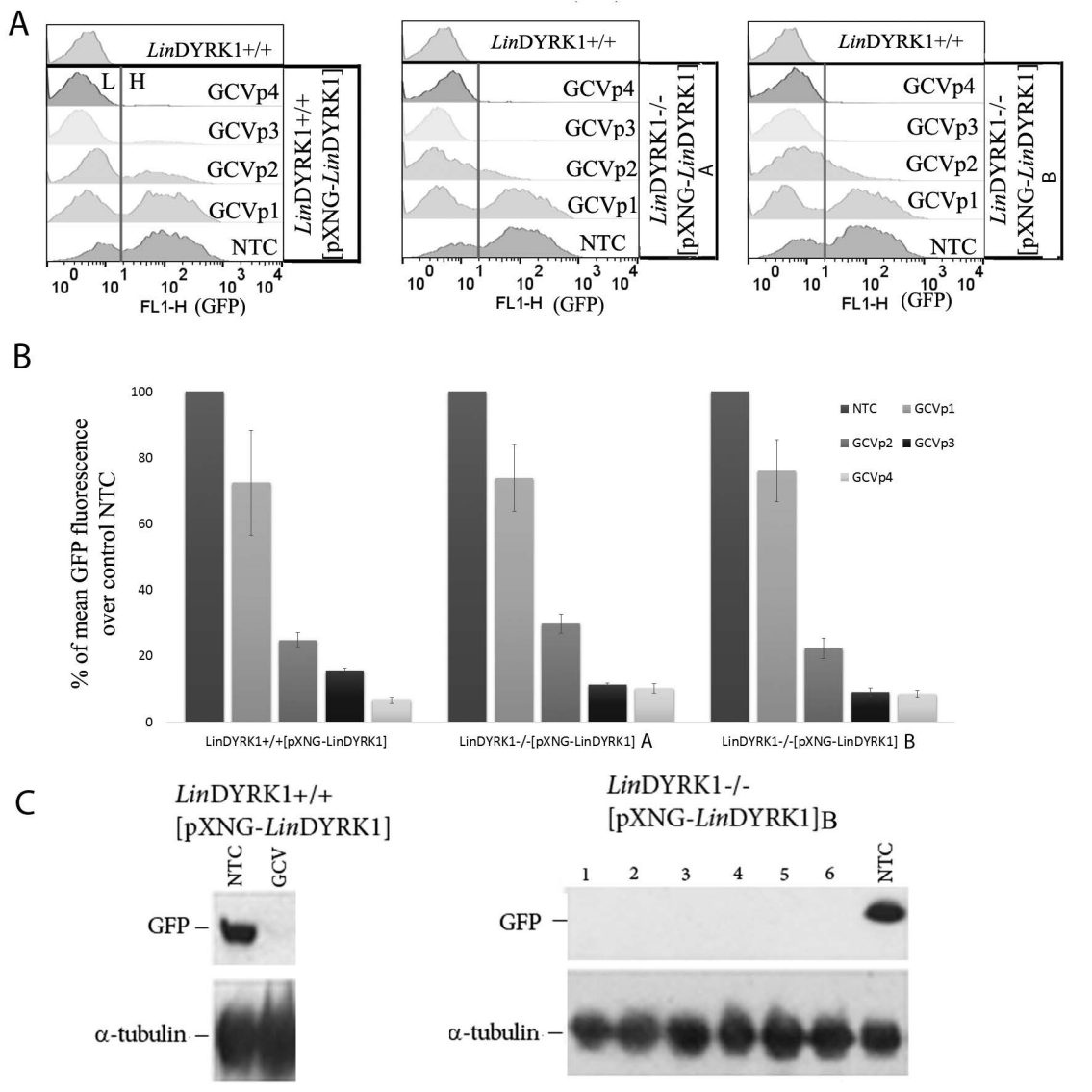
A
LinDYRK1+/+
L
H
GCVp4
GCVp3
GCVp2
GCVp1
NTC
LinDYRK1+/+ [pXNG-LinDYRK1]
LinDYRK1-/- [pXNG-LinDYRK1] A
LinDYRK1-/- [pXNG-LinDYRK1] B
FL1-H (GFP)
B
% of mean GFP fluorescence over control NTC
LinDYRK1+/+[pXNG-LinDYRK1]
LinDYRK1-/-[pXNG-LinDYRK1] A
LinDYRK1-/-[pXNG-LinDYRK1] B
C
LinDYRK1+/+ [pXNG-LinDYRK1]
NTC
GCV
GFP
α-tubulin
LinDYRK1-/- [pXNG-LinDYRK1]B
1
2
3
4
5
6
NTC

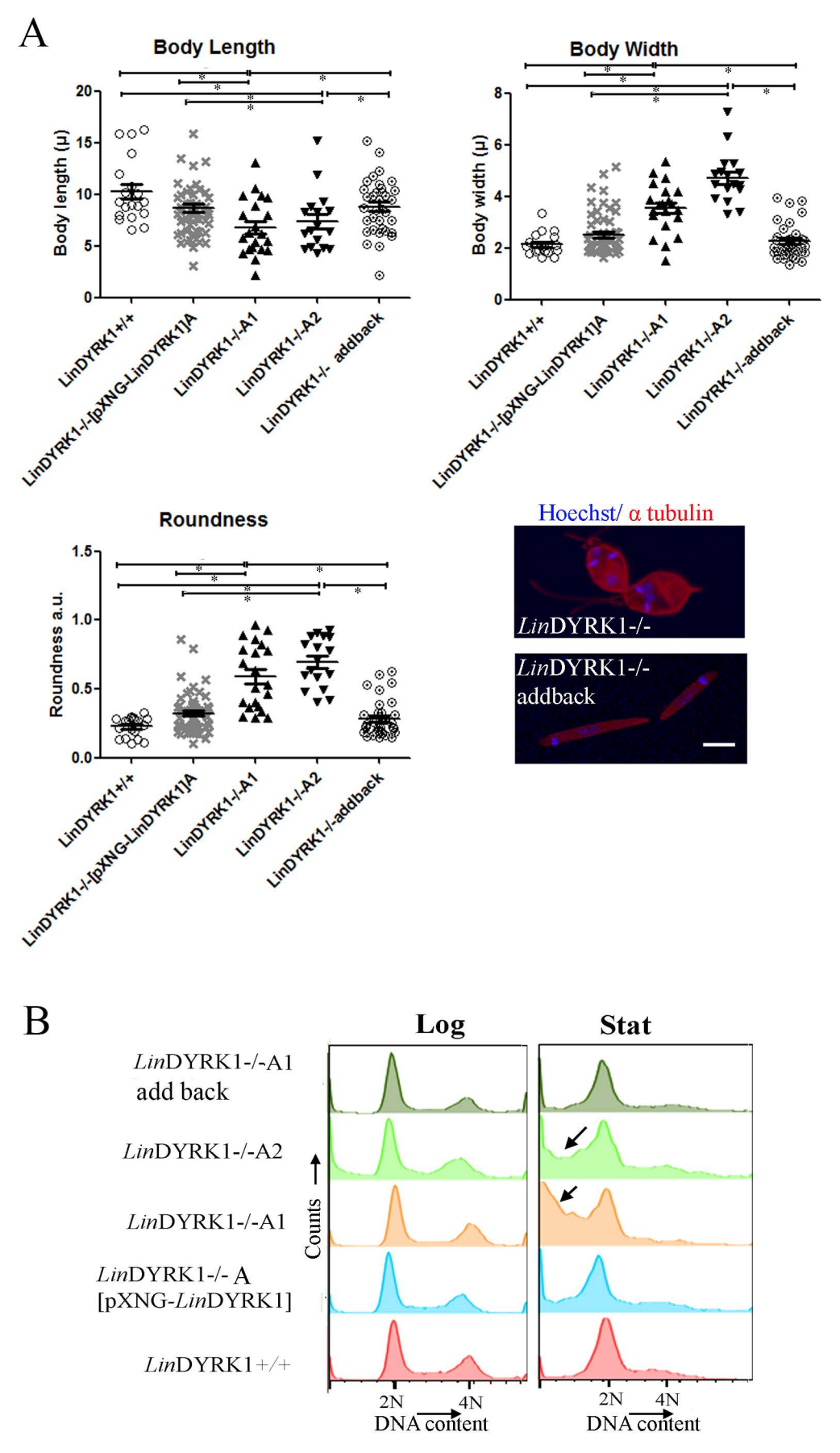
A
Body Length
Body length (μ)
20
15
10
5
0
LinDYRK1+/+
LinDYRK1-/-[pXNG-LinDYRK1]A
LinDYRK1-/-A1
LinDYRK1-/-A2
LinDYRK1-/- addback
Body Width
Body width (μ)
8
6
4
2
0
LinDYRK1+/+
LinDYRK1-/-[pXNG-LinDYRK1]A
LinDYRK1-/-A1
LinDYRK1-/-A2
LinDYRK1-/-addback
Roundness
Roundness a.u.
1.5
1.0
0.5
0.0
LinDYRK1+/+
LinDYRK1-/-[pXNG-LinDYRK1]A
LinDYRK1-/-A1
LinDYRK1-/-A2
LinDYRK1-/-addback
Hoechst/ α tubulin
LinDYRK1-/-
LinDYRK1-/-
addback
B
Log
Stat
LinDYRK1-/-A1
add back
LinDYRK1-/-A2
LinDYRK1-/-A1
LinDYRK1-/- A
[pXNG-LinDYRK1]
LinDYRK1+/+
Counts
2N
4N
DNA content
2N
4N
DNA content

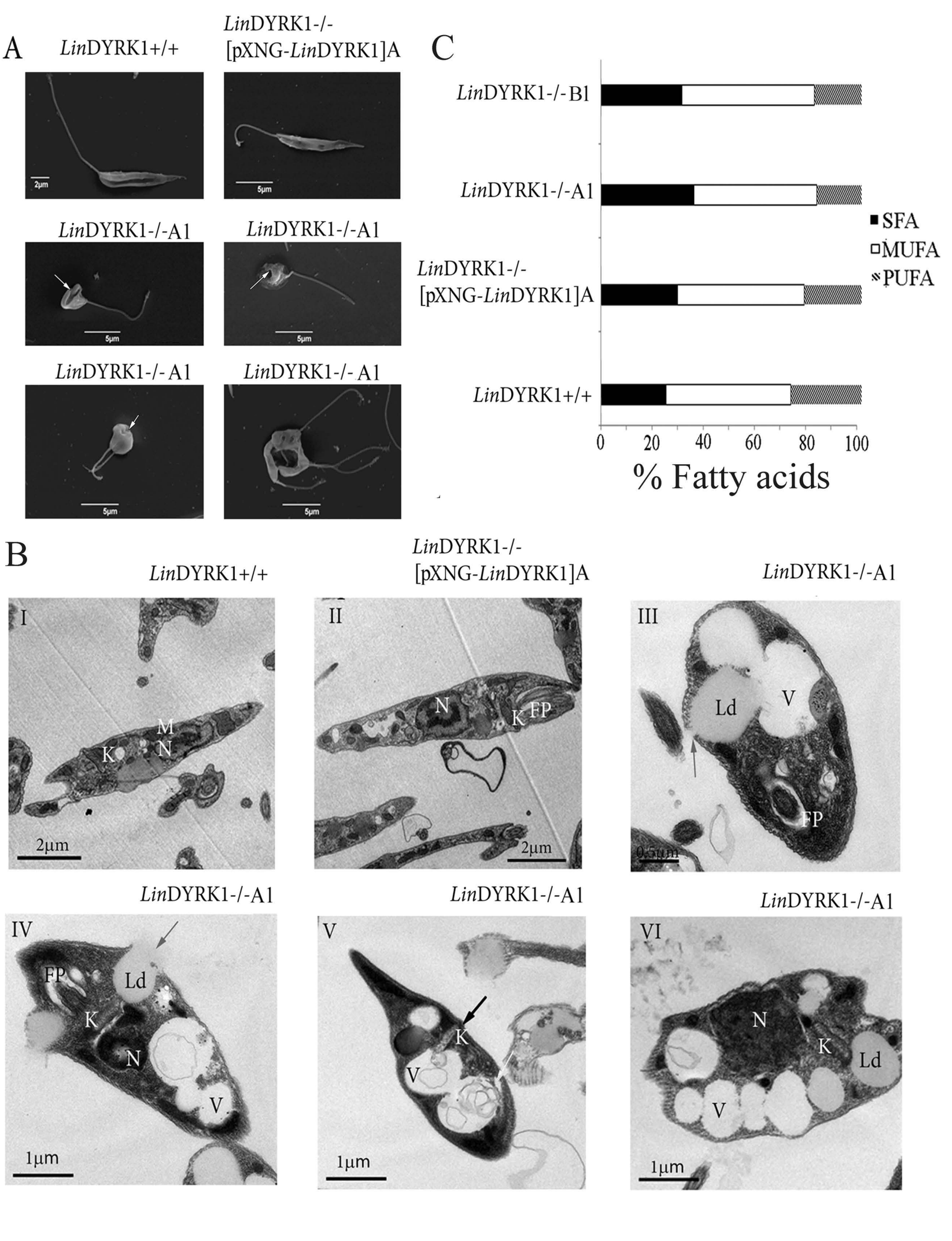
A
LinDYRK1+/+
LinDYRK1-/-
[pXNG-LinDYRK1]A
LinDYRK1-/-A1
LinDYRK1-/-A1
LinDYRK1-/- A1
LinDYRK1-/- A1
2µm
5µm
C
LinDYRK1-/- B1
LinDYRK1-/-A1
LinDYRK1-/-
[pXNG-LinDYRK1]A
LinDYRK1+/+
SFA
MUFA
PUFA
0
20
40
60
80
100
% Fatty acids
B
LinDYRK1+/+
LinDYRK1-/-
[pXNG-LinDYRK1]A
LinDYRK1-/-A1
I
M
K
N
2µm
II
N
K
FP
2µm
III
Ld
V
FP
0.5µm
LinDYRK1-/-A1
LinDYRK1-/-A1
LinDYRK1-/-A1
IV
FP
Ld
K
N
V
1µm
V
K
V
1µm
VI
N
K
Ld
V
1µm

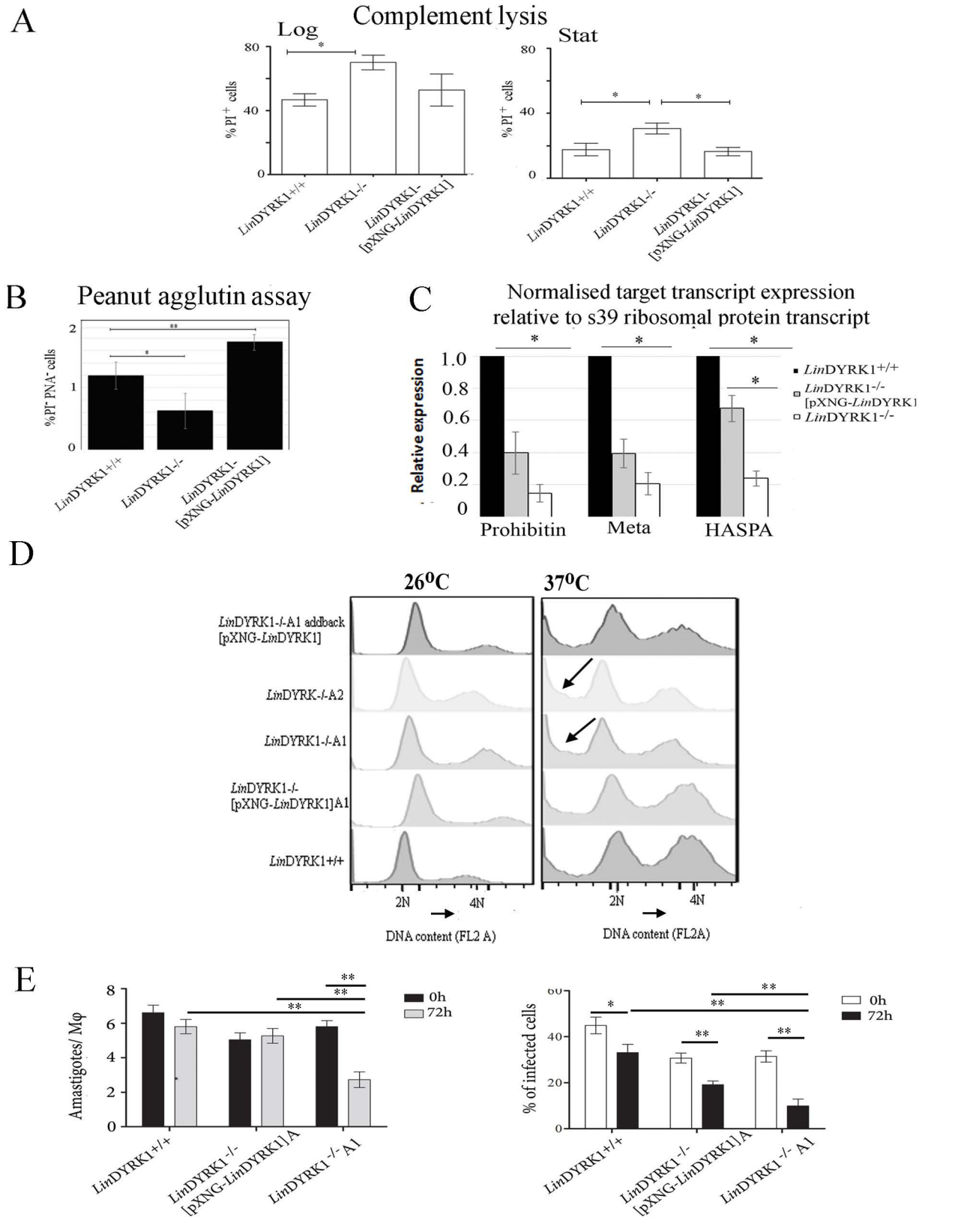
A
Complement lysis
Log
Stat
% PI+ cells
80
40
0
LinDYRK1+/+
LinDYRK1-/-
LinDYRK1-[pXNG-LinDYRK1]
B
Peanut agglutin assay
%PI- PNA- cells
2
1
0
C
Normalised target transcript expression relative to s39 ribosomal protein transcript
Relative expression
1.0
0.8
0.6
0.4
0.2
0
Prohibitin
Meta
HASPA
LinDYRK1+/+
LinDYRK1-/- [pXNG-LinDYRK1]
LinDYRK1-/-
D
26⁰C
37⁰C
LinDYRK1-/-A1 addback [pXNG-LinDYRK1]
LinDYRK-/-A2
LinDYRK1-/-A1
LinDYRK1-/- [pXNG-LinDYRK1]A1
LinDYRK1+/+
2N
4N
DNA content (FL2 A)
DNA content (FL2A)
E
Amastigotes/ Mφ
0h
72h
LinDYRK1+/+
LinDYRK1-/- [pXNG-LinDYRK1]A
LinDYRK1-/- A1
% of infected cells

Leishmania dual-specificity tyrosine-regulated kinase 1 (DYRK1) is required for sustaining *Leishmania* stationary phase phenotype

Vinícius Pinto Costa Rocha[1] , Mariko Dacher[2#a], Simon Alan Young[3], Foteini Kolokousi[4], Antonia Efstathiou[4], Gerald Frank Späth[2], Milena Botelho Pereira Soares[1]*, Despina Smirlis[4]*

[1]Instituto Gonçalo Moniz, Fundação Oswaldo Cruz (FIOCRUZ), Rua Waldemar Falcão 121, Salvador, BA, Brazil;

[2]Unité de Parasitologie Moléculaire et Signalisation, Department of Parasites and Insect Vectors, Institut Pasteur and INSERM U1201, Paris, France;

[3]Biomedical Sciences Research Complex, School of Biology, The University of St. Andrews, North Haugh, St. Andrews, Fife, Scotland, UK;

[4]Molecular Parasitology Laboratory, Microbiology Department, Hellenic Pasteur Institute, 127 Bas. Sofias Avenue, Athens, Greece;

[#a]Current address: Laboratory of Chromatin Structure and Function, Institute for Quantitative Biosciences, The University of Tokyo, Yayoi 1-1-1, Bunkyo-ku, Tokyo, Japan.

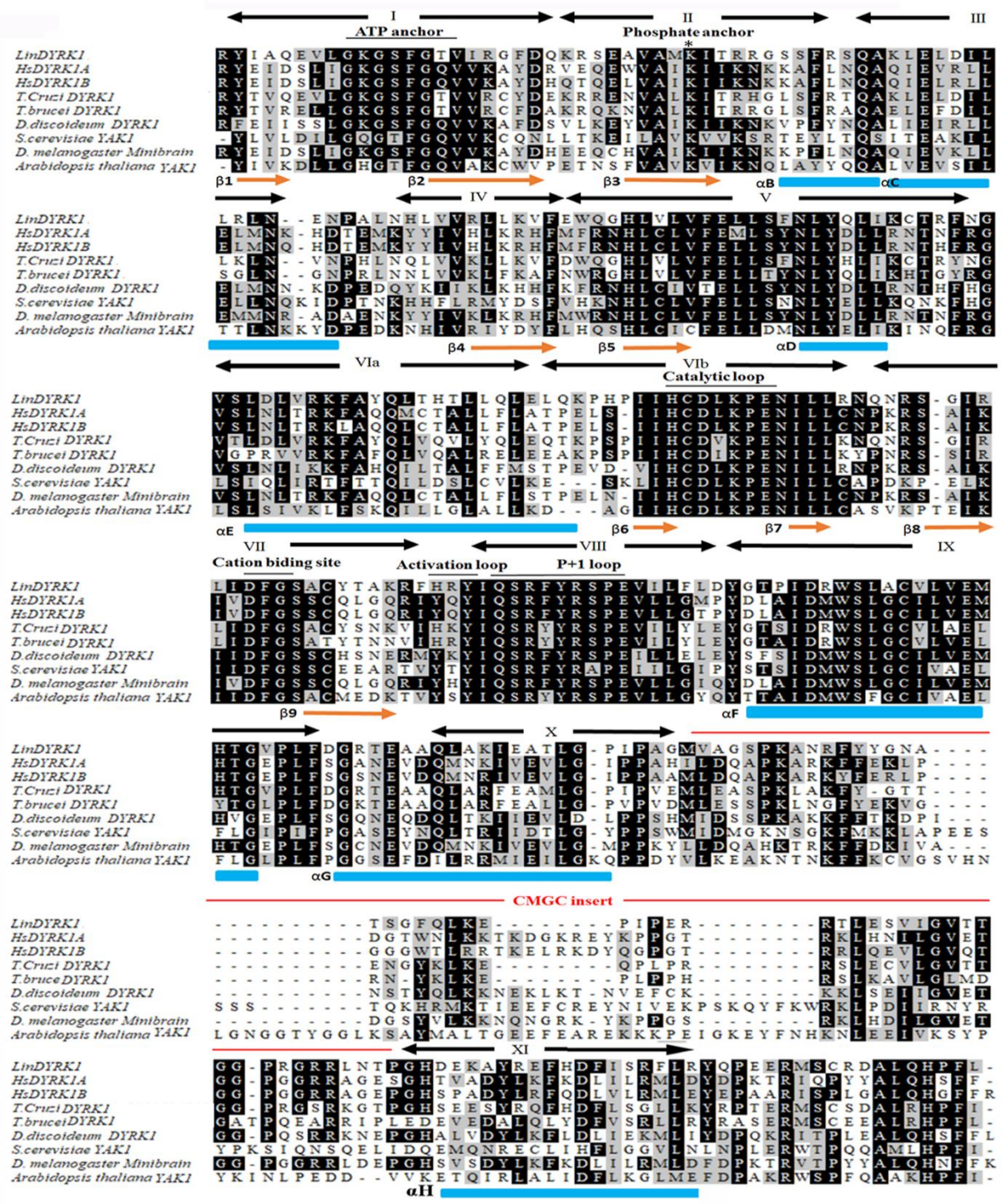

S1 Fig. Kinase domain alignement of DYRK1 and related kinases from different organisms.

Alignment of the kinase domains of DYRK1 kinases and Yaks syntenic trypanosomatid DYRK1s [*T. cruzi DYRK1* (A0A422PWG1), *T. brucei DYRK1 (*AAZ11280)], of the *H. sapiens*

(Hs) DYRK1A (Q13627) and HsDYRK1B (Q9Y463), of *S. cerevisiae YAK1* (P14680), *D. discoideum DYRK1* (Q76NV1) and of *D. melanogaster Minibrain* (P49657). Identical aminoacids are shaded in black and similar in grey. Secondary structure predictions (α helix blue, β sheet orange) of the kinase domains correspond to the DYRK1A kinase domain (http://www.rcb.org/pdb/home.home.do). Lines indicate kinase subdomains (I-XI), according to Hanks and Hunter (Hanks & Hunter, 1995) and functional features including the ATP anchor, phosphate anchor, catalytic loop, cation binding site, activation loop, P+1 loop and CMGC insert (red line).

S2 Fig

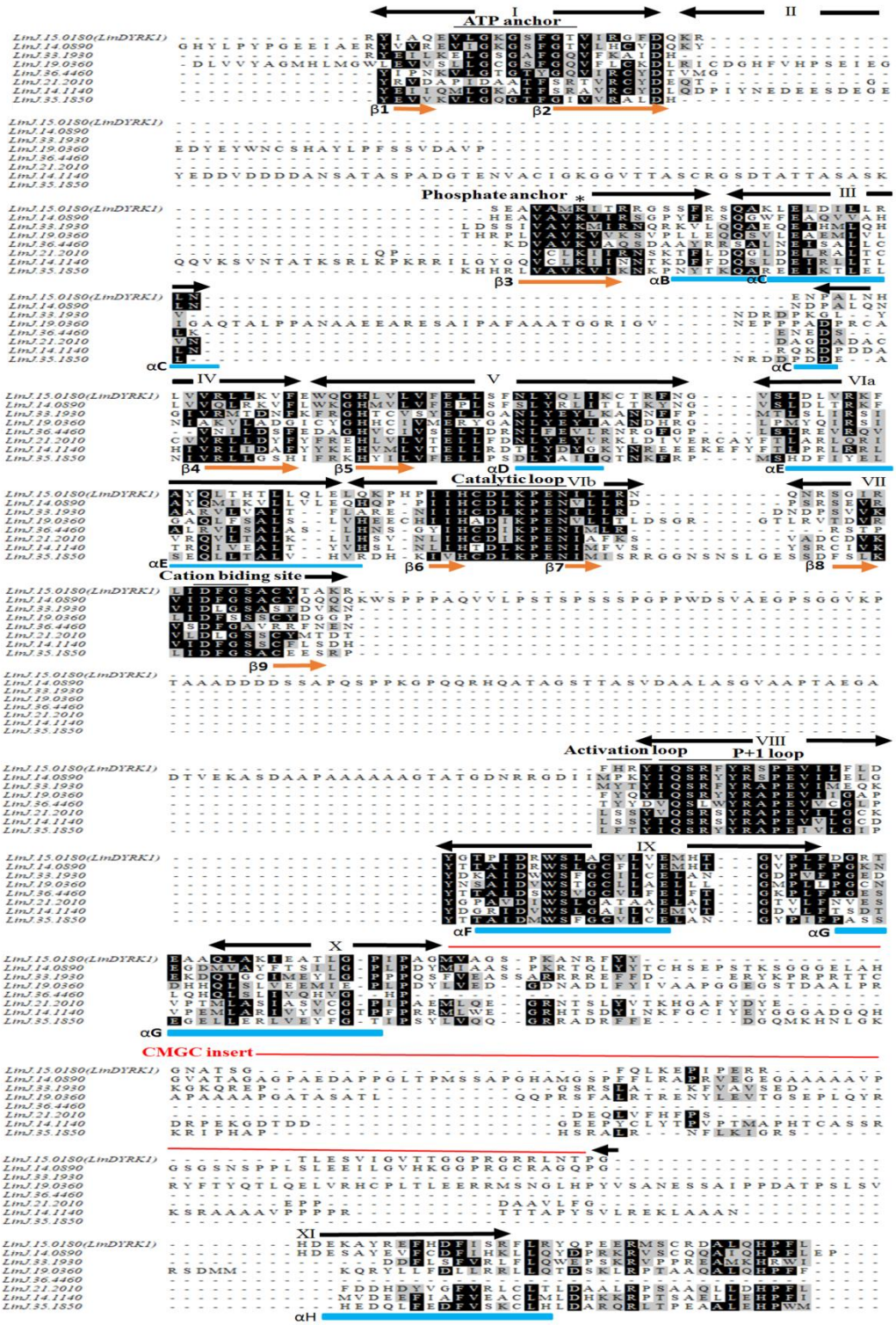

S2 Fig. Multiple sequence alignment. Protein sequence alignment of the kinase domain of the eight *L. infantum* DYRKs using CLUSTALW as described in "Materials and Methods". Identical amino acids are shaded in black and similar in grey. Secondary structure

predictions (α helix blue, β sheet orange) of the kinase domains correspond to the DYRK1A kinase domain (http://www.rcb.org/pdb/home.home.do). Lines indicate kinase subdomains (I-XI) according to Hanks and Hunter (Hanks & Hunter, 1995) and functional features including the ATP anchor, phosphate anchor, catalytic loop, cation binding site, activation loop, P+1 loop and CMGC insert (red line).

Fig. S3

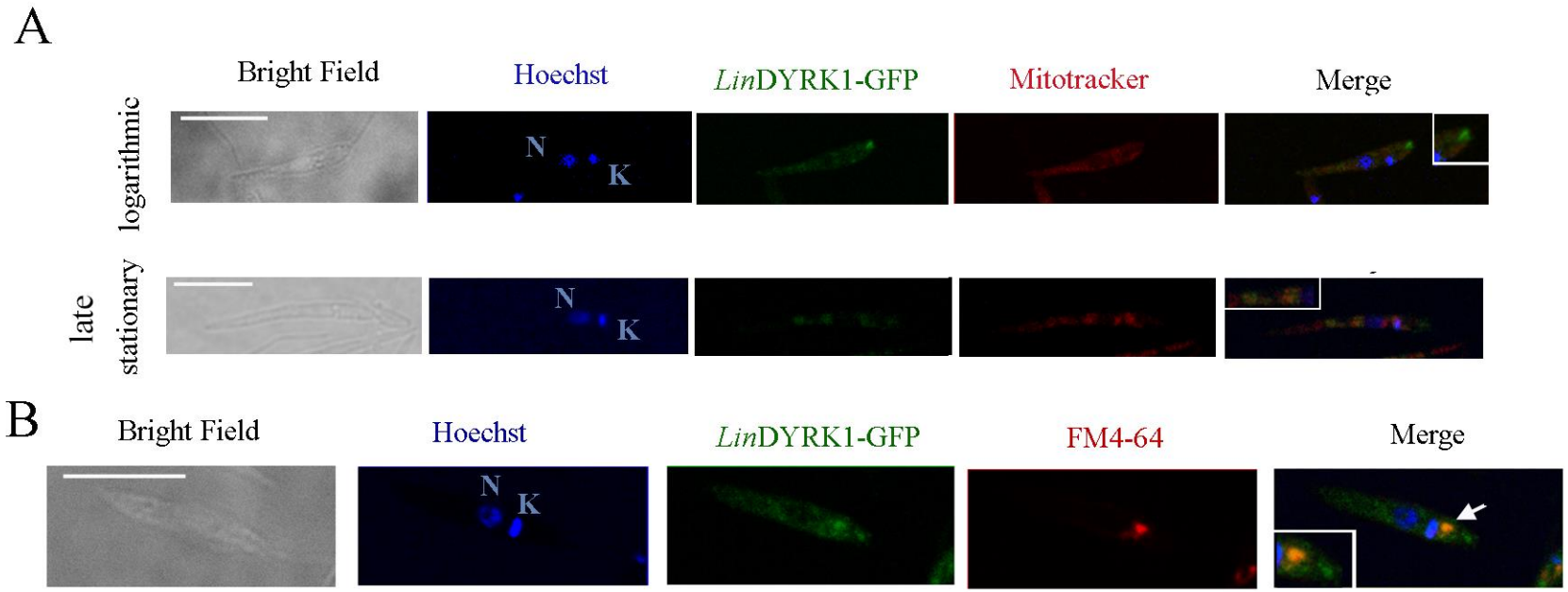

S3 Fig. Localisation of *Lin*DYRK1-GFP. Fluorescence confocal microscopy showing the localisation of the *Lin*DYRK1-GFP hybrid protein (*Lin*DYRK1-GFP, green) in logarithmic (scale bar = 5 μm), and late stationary promastigotes (scale bar= 5 μm). Promastigotes were stained with mitotracker (mitotracker, red) to visualise the mitochondrion and Hoechst 33342 (Hoechst, blue) to visualise the nucleus (N) and kinetoplast (K). Bright field and images with merged channels are also shown. (C) Fluorescence confocal microscopy showing the localisation of the GFP-*Lin*DYRK1 hybrid protein (*Lin*DYRK1-GFP, green) in logarithmic cells stained with FM®4-64FX (FM4-64, Red) (pulse chase experiment) for20

90 min at 4°C to visualise the endosomal compartment and Hoechst 33342 (Hoechst, blue) to visualise the nucleus (N) and kinetoplast (K). Bright
91 field and images with merged channels are also shown Scale bar= 5 μm, Insets: 1.5 fold magnificati

Supporting information

S4 Fig

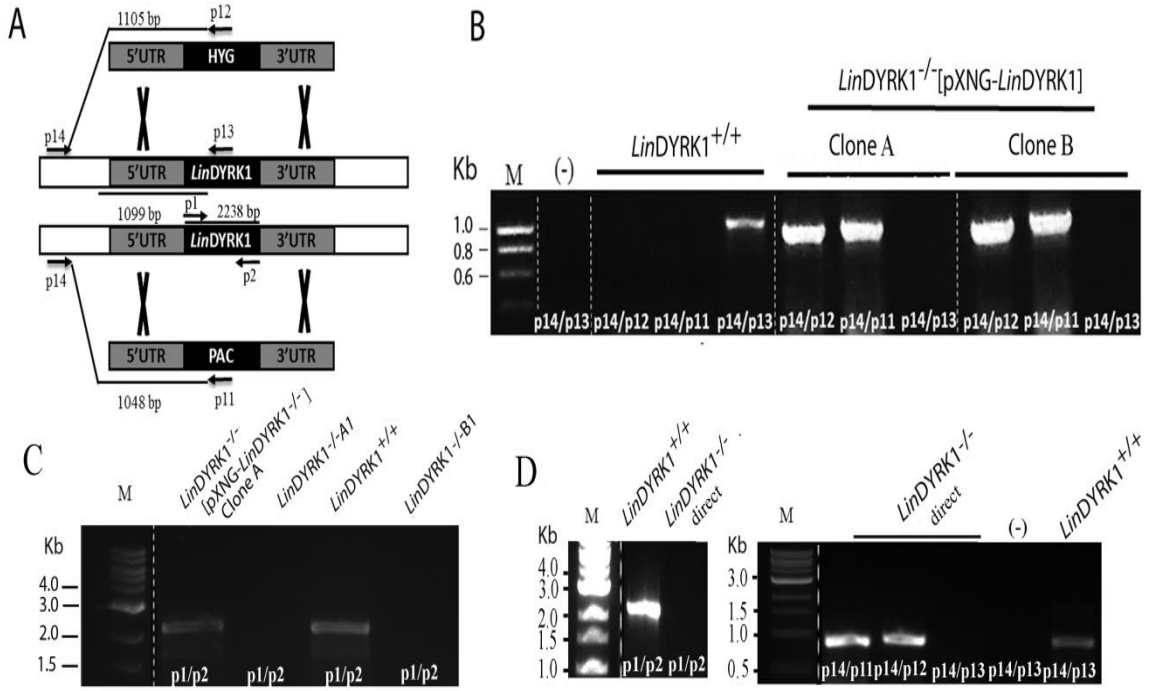

S4 Fig. Generation of *Lin*DYRK1 facilitated null mutants. (A) Schematic representation showing the genomic structure of *Lin*DYRK1 and the gene replacement strategy. The two alleles of *Lin*DYRK1 were replaced by HYG and PAC resistance cassettes yielding homozygous facilitated null mutants in *Lin*DYRK1$^{-/-}$[pXNG-*Lin*DYRK1] (facilitated) or in wild type *Lin*DYRK1$^{+/+}$ cells. The primers sets used for PCR amplifications and the predicted sizes of the PCR products in base pairs (bp) are indicated. (B) Diagnostic PCR to evaluate the establishment of facilitated knockouts generating independent clones *Lin*DYRK1$^{-/-}$[pXNG-*Lin*DYRK1]**A** and **B**. PCR analysis from wild type *Lin*DYRK1$^{+/+}$ genomic DNA is used as well as a negative control a PCR reaction with no DNA (-). The DNA marker with the band sizes indicated is also presented (M). The size of the expected amplicons is indicated in Panel A. (C) Diagnostic PCR to evaluate the presence of an endogenous *Lin*DYRK1 copy with the use of internal primers p1/p2, after the loss of the pXNG-*Lin*DYRK1 episome in *Lin*DYRK1$^{-/-}$**A1** and *Lin*DYRK1$^{-/-}$**B1** mutants. As a control wild type promastigotes (*Lin*DYRK1$^{+/+}$) and *Lin*DYRK1$^{-/-}$[pXNG-*Lin*DYRK1] were also

included. The DNA marker with the band sizes indicated is also presented (M). (D) Diagnostic PCR to evaluate to evaluate the establishment of conventional knockout clone (*Lin*DYRK1$^{-/-}$ direct). Right panel: Primer pairs p11/p14 and p12/p14 were used to validate the placement of the PAC and HYG cassettes respectively in *Lin*DYRK1$^{-/-direct}$ mutants. The p13/p14 primer set was also used to validate the presence of an extra genomic copy of *Lin*DYRK1 within the DYRK1 genomic locus. As a positive control PCR analysis is performed with primer sets p13/14 and as negative control PCR reaction with no DNA (-). The DNA marker with the band sizes indicated is also presented (M). Left Panel: Diagnostic PCR to validate the absence of any genomic *Lin*DYRK1 copy outside the *Lin*DYRK1 locus in *Lin*DYRK1$^{-/-direct}$ mutants. Primer set p1/p2 was used to establish the absence of endogenous copy of *Lin*DYRK1 in *Lin*DYRK1$^{-/-direct}$ mutants (*Lin*DYRK1-/-direct). As a positive control analysis of wild type (*Lin*DYRK1$^{+/+}$) genomic DNA was performed. (-). The DNA marker with the band sizes indicated is also presented (M).

Supporting information

S5 Fig

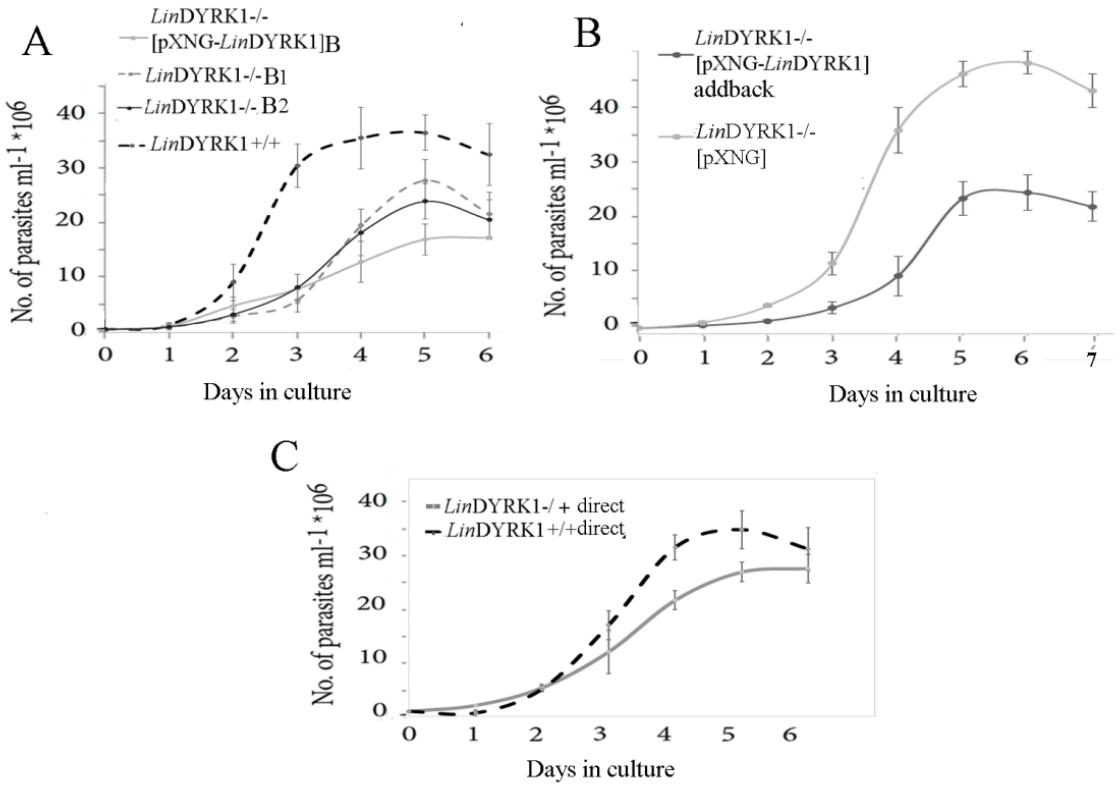

S5 Fig. *Lin*DYRK1$^{-/-}$ growth curves (A) Growth curves of *Lin*DYRK1$^{-/-}$**B1** and *Lin*DYRK1$^{-/-}$**B2** with respect to the parental clone *Lin*DYRK1$^{-/-}$[pXNG-*Lin*DYRK1]**B1** and to wild type cells. Growth of parasites was monitored daily by cell count followed for six days. Error bars show standard deviation of 5 different experiments. (B) Growth curves of *Lin*DYRK$^{-/-}$[pXNG] (clone A1) and *Lin*DYRK$^{-/-}$[pXNG-*Lin*DYRK1] addbacks (clone A1).Growth of parasites was monitored daily by cell count followed for seven days. Error bars show standard deviation of 4 different experiments. (C) Growth curve of conventional mutant *Lin*DYRK1$^{-/-}$ (*Lin*DYRK1$^{-/-direct}$) with respect to its heterozygous parental clone *Lin*DYRK1$^{+/-}$ (*Lin*DYRK1$^{+/-direct}$), and wild type promastigotes (*Lin*DYRK1$^{+/+}$). Error bars show standard deviation of 4 different experiments.

Supporting information

S6 Fig

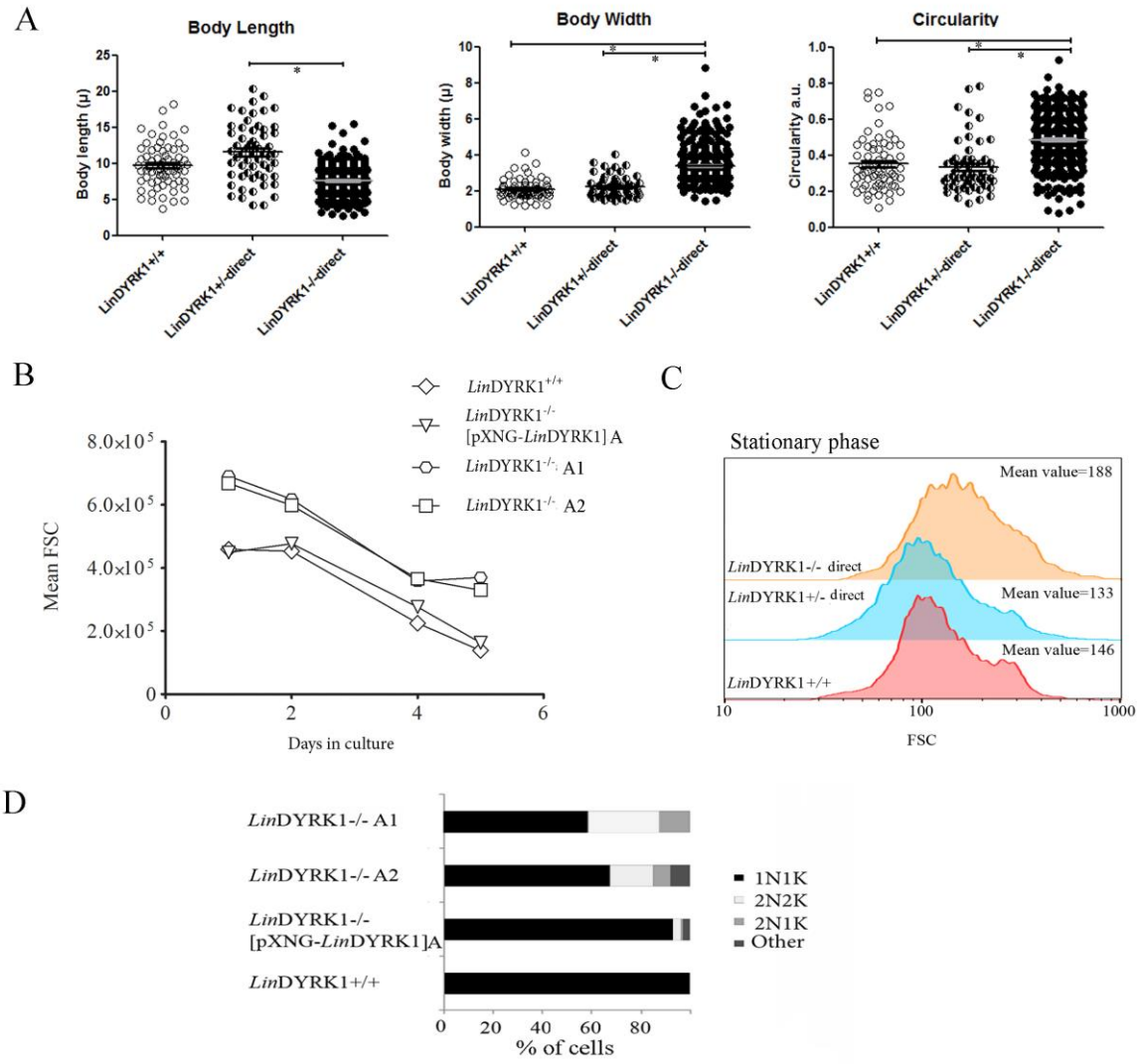

S6 Fig. Morphology and DNA content of *Lin*DYRK1$^{-/-}$ stationary parasites (A) Morphometric measurements showing roundness, body length and body width of *Lin*DYRK1$^{-/-}$ direct, *Lin*DYRK1$^{+/-direct}$ and *Lin*DYRK1$^{+/+}$ wild type cells. Bars represent mean ± error. * Statistically significant ($p < 0.05$). (B) The forward scatter (FSC) was analysed as an estimation of cell size/morphology by flow cytometry in *Lin*DYRK1$^{-/-}$**A1**, *Lin*DYRK1$^{-/-}$**A2** and their comparison to wild type *Lin*DYRK1$^{+/+}$ and parental clone *Lin*DYRK1$^{-/-}$[pXNG-*Lin*DYRK]**A**. The

figure represents the mean FSC of 10,000 events per each cell line. (C) FSC histogram plots of *Lin*DYRK1$^{-/-direct}$ (orange), *Lin*DYRK1$^{+/-direct}$ (blue) and wild type *Lin*DYRK1$^{+/+}$ (red) promastigotes in mid stationary phase. Mean value is shown for 10,000 events. (D) Nuclear and kinetoplast DNA content analysis of mid stationary promastigotes (25-40 *10^6 mL^{-1}). Nuclei and kinetoplasts of at least 50 parasites per clone were counted.

Supporting information

178 **S7 Fig**

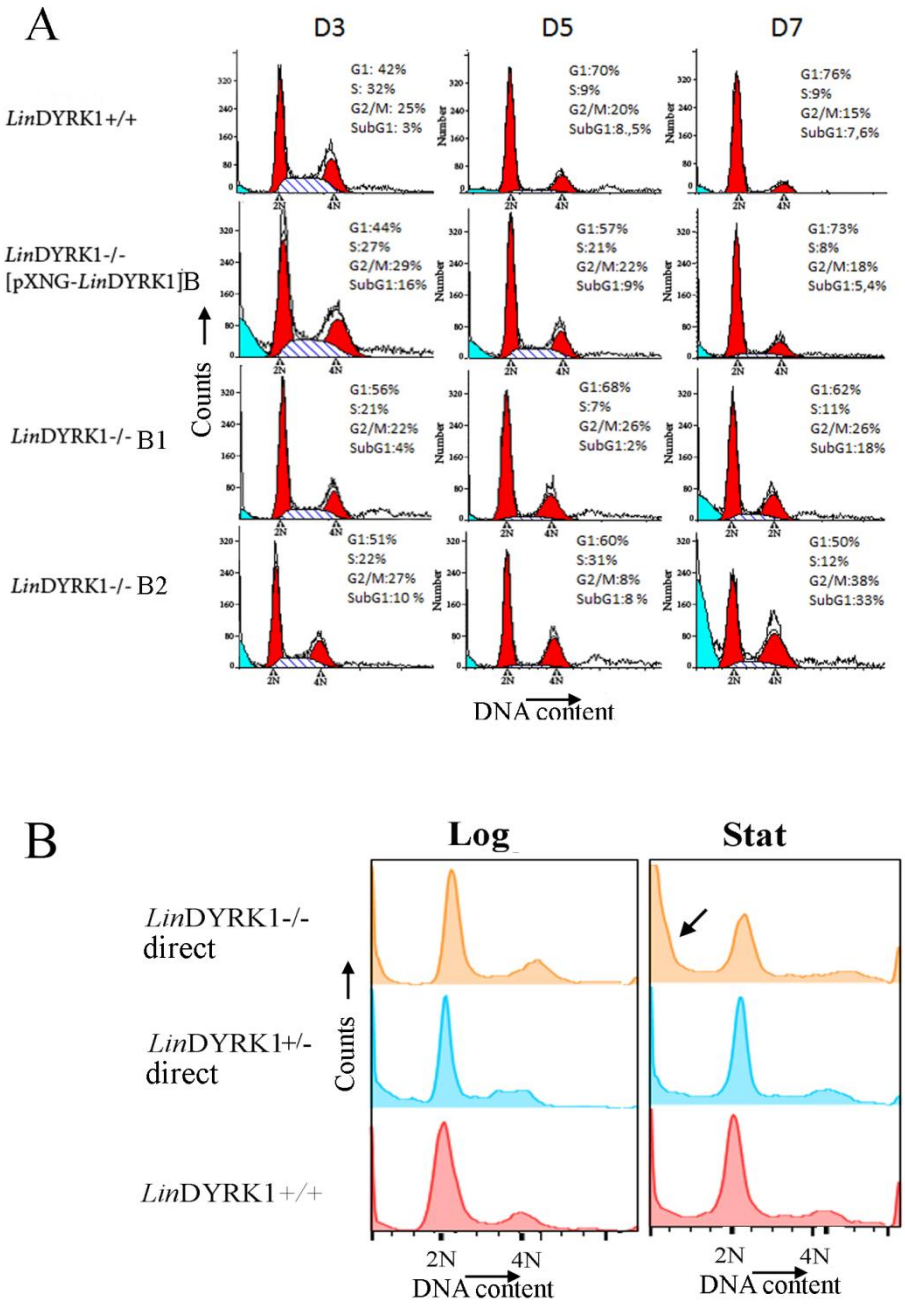

179

180 **S7 Fig. Cell cycle analysis of *Lin*DYRK1$^{-/-}$ mutants at different days of cell culture. (A)** Cell
181 cycle analysis of wild type *Lin*DYRK1$^{+/+}$, parental *Lin*DYRK1$^{-/-}$ [pXNG-*Lin*DYRK1]**B** pool and
182 two *Lin*DYRK1$^{-/-}$**B** clones (*Lin*DYRK1$^{-/-}$**B1** and *Lin*DYRK1$^{-/-}$**B2**). Cell cycle analysis was
183 performed on day 3 (logarithmic), day 5 (mid stationary phase), and day 7 (late stationary phase

promastigotes). Diploid (2N) and tetraploid (4N) DNA content is indicated. Cell cycle distribution is presented on the right hand side of each image. This analysis is representative of three independent culture experiments. (B) Cell cycle analysis of wild type *Lin*DYRK1$^{-/-direct}$, parental heterozygous and wild type cells in logarithmic (Log) and late stationary phase (Stat) Diploid (2N) and tetraploid (4N) DNA content is indicated. Cell cycle distribution is presented on the right hand side of each image. Arrow represents a great increase in hypodiploid DNA content. This analysis is representative of three independent culture experiments.

S8 Fig

Supporting information

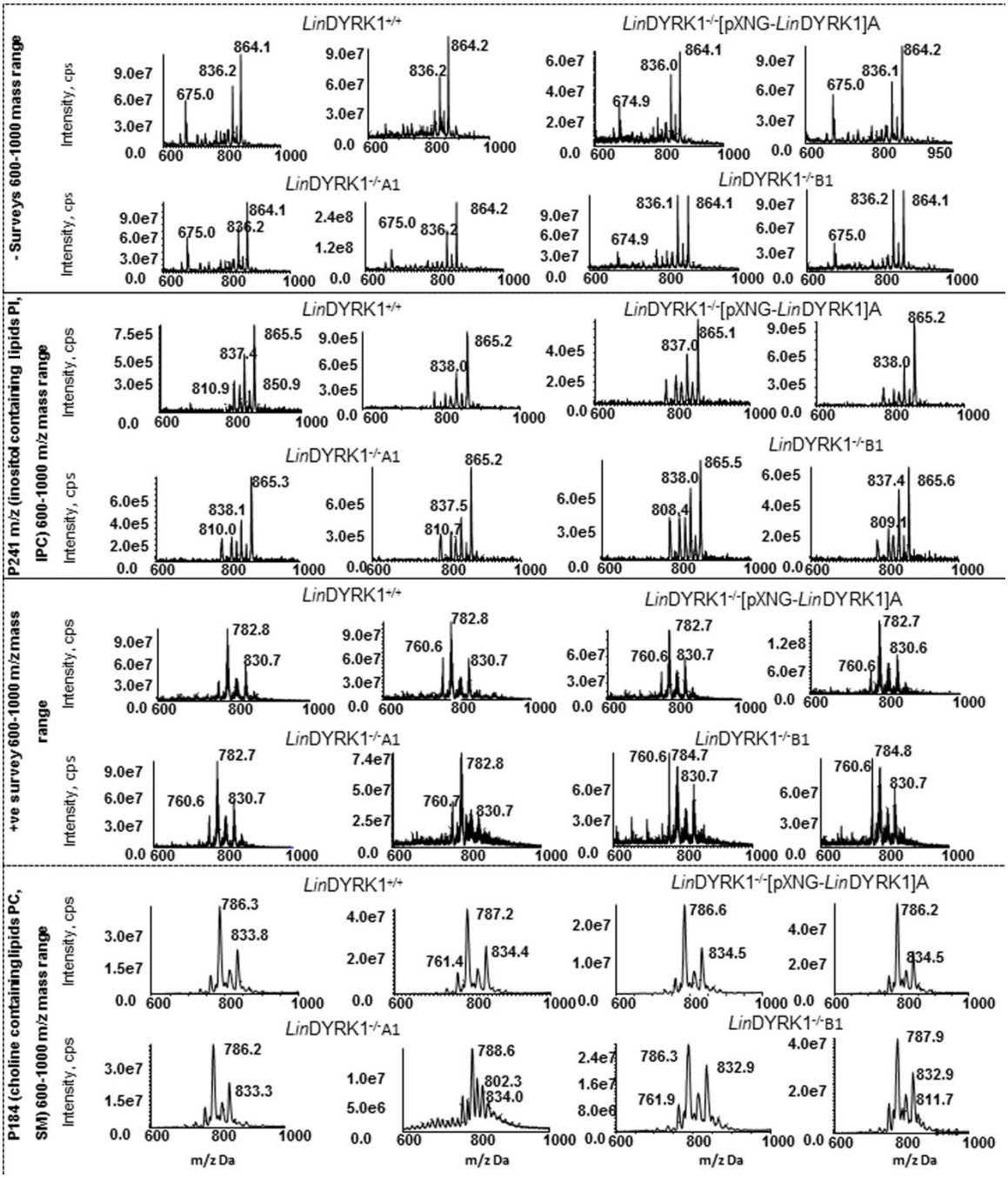

S8 Fig. Phospholipid analysis Lipids isolated from *Lin*DYRK1$^{+/+}$, *Lin*DYRK1$^{-/-}$[pXNG-*Lin*DYRK1]**B**, *Lin*DYRK1$^{-/-}$**B** and *Lin*DYRK1$^{-/-}$**B** in stationary phase were analysed in both positive and negative ion modes. Tandem mass spectra (MS/MS) were obtained for phosphatidylinositol (PI)/inositol-phosphoceramide (IPC) species in negative ion mode (parent-

ion scanning of m/z 241); and phosphatidylcholine (PC)/sphingomyelin (SM) species in positive mode (parent-ion scanning of m/z 184).

S9 Fig

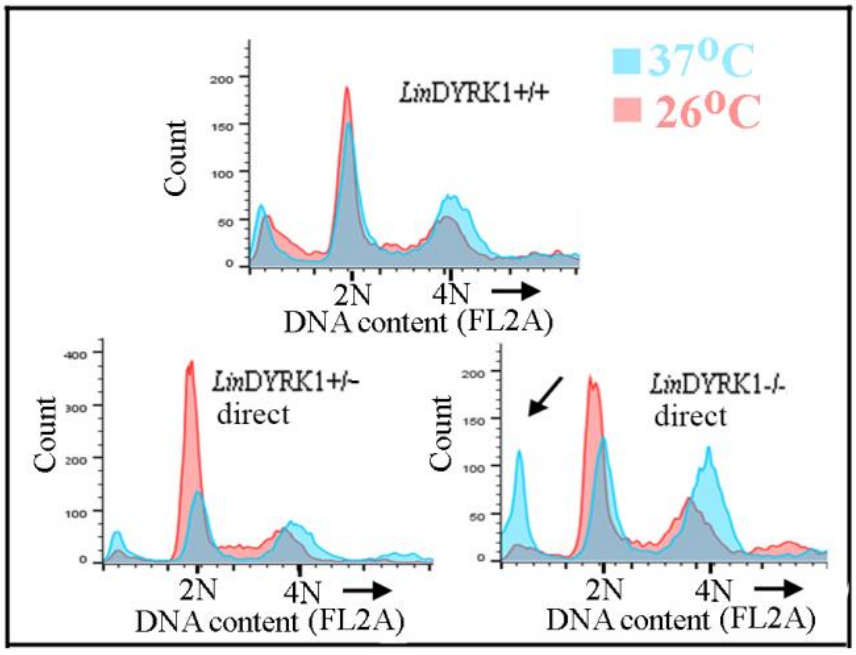

S9 Fig. Cell cycle analysis of *Lin*DYRK1$^{-/-direct}$ promastigotes under heat-shock. Overlaid histograms plots showing the DNA content (FL2A) of logarithmic *Lin*DYRK1+/+, *Lin*DYRK1$^{+/-direct}$, *Lin*DYRK1$^{-/-direct}$ cultivated at 26°C (pink) and 37°C (blue) for 16 h. Diploid (2N) and tetraploid (4N) DNA content is indicated. Results are representative of 3 experiments. Black arrow show the increased percentage of hypodiploid cells.

Supporting information

S1 Table: Cell cycle distribution of *LinDYRK1*$^{+/+}$[pXNG-*Lin*DYRK] and *LinDYRK1*$^{+/+}$[pXNG] cells after HU withdrawal.

	Cell cycle distribution after synchronisation								
	0 h			3 h			6.5 h		
	G1	S	G_2/M	G1	S	G_2/M	G1	S	G_2/M
***Lin*DYRK1$^{+/+}$[pXNG]**	71	11	17	61	21	18	15	20	65
***Lin*DYRK1$^{+/+}$[pXNG-*Lin*DYRK1]**	76	9	15	70	15	15	51	39	10

Percentage of cell cycle phases *Lin*DYRK1$^{+/+}$[pXNG] and *Lin*DYRK1$^{+/+}$[pXNG-*Lin*DYRK1] 0 h, 3 h and 6.5 h post hydroxyurea release. This is one representative of three experiments.

S2 Table: Cell cycle distribution of *Lin*DYRK1$^{-/-}$ mutants and control cells parasites in logarithmic, stationary phase and in heat-shock

A.		**CELL CYCLE ANALYSIS OF FACILITATED *Lin*DYRK1$^{-/-}$ MUTANTS AND *Lin*DYRK1-/- ADDBACK COMPARISON IN LOGARITHMIC AND STATIONARY CELL CULTURE GROWTH PHASE**				
		***Lin*DYRK1$^{+/+}$**	***Lin*DYRK1$^{-/-}$ [pXNG-*Lin*DYRK1]**A	***Lin*DYRK1$^{-/-}$**A1	***Lin*DYRK1$^{-/-}$** A2	***Lin*DYRK1$^{-/-}$ ADDBACK**
Log (% phases)	**SubG1**	2	3.1	2.2	11	1.8
	G1	49.9	54	52.3	56.8	60.7
	S	13.1	12.6	9.7	12	8.7
	G2/M	34.7	29.6	35.6	29.9	28.6
Stat (% phases)	**SubG0/G1**	4.9	15.2	46.3	33.8	9.4
	G1	70.9	59.5	43.6	42.6	64.8
	S	7.1	6.8	4.3	5.8	5.5
	G2/M	17.7	18.1	5.6	17.5	20.1

B.		**CELL CYCLE ANALYSIS OF *Lin*DYRK1$^{-/-\ direct}$ MUTANTS IN LATE LOGARITHMIC AND STATIONARY CELL CULTURE GROWTH PHASE**		
		***Lin*DYRK1$^{+/+}$**	***Lin*DYRK1$^{+/-direct}$**	***Lin*DYRK1$^{-/-direct}$**
Log (% phases)	**SubG0 /G1**	4.4	15.9	9.9
	G1	68.9	52.6	59.6
	S	10	13.9	12.3
	G2/M	16.5	17.4	18

Supporting information

Stat (% phases)	**SubG0/G1**	11.5	16.9	49.2
	G1	55.4	56	34.5
	S	14.6	8.5	5.5
	G2/M	18.2	18.5	5.7

C.		**CELL CYCLEANALYSIS OF FACILITATED *Lin*DYRK1$^{-/-}$ MUTANTS AND *Lin*DYRK1-/- ADDBACK COMPARISON AT 26 ºC AND 37ºC**				
		***Lin*DYRK1$^{+/+}$**	***Lin*DYRK1$^{-/-}$ [pXNG-*Lin*DYRK1]** A	***Lin*DYRK1$^{-/-}$**A1	***Lin*DYRK1$^{-/-}$**A2	***Lin*DYRK1$^{-/-}$**A1[pXNG-*Lin*DYRK1] addback
T=26ºC (% phases)	**SubG0/G1**	6.7	4.6	1.45	4.8	3.5
	G1	63.4	61.7	53.8	47.2	63.6
	S	9.8	12.4	11.5	14.7	8.5
	G2/M	19.9	21.1	33.21	33.1	24.2
T=37ºC (% phases)	**SubG1**	12.5	17.1	29.03	28.0	16.12
	G1	35.9	33.7	29.03	38.5	38.0
	S	11.3	12.11	10.7	7.8	11.6
	G2/M	40.2	6.9	31.1	25.4	34.1

D.		**CELL CYCLE ANALYSIS OF *Lin*DYRK1$^{-/-\ direct}$ MUTANTS AT 26 ºC AND 37ºC**		
		***Lin*DYRK1$^{+/+}$**	***Lin*DYRK1$^{+/-direct}$**	***Lin*DYRK1$^{-/-direct}$**
T=26ºC (% phases)	**SubG1**	22	5.5	7.5
	G1	42.8	57.7	53
	S	10.5	11.6	6.8
	G2/M	25.7	18.2	32
T=37ºC (% phases)	**SubG1**	15.8	15.6	24.5
	G1	41.5	40.5	29
	S	6.5	5.8	4.5
	G2/M	39	38	42

Percentages of cell cycle phases in logarithmic, stationary growth phase and during a 16 h 26→37 ºC heat-shock are shown.

S3 Table: List of DYRK sequences used for the phylogenetic analysis

Protein name	**Species**	**Accession number**
Yak1p	*Saccharomyces cerevisiae*	NP_012394; GI:6322320
Pom1p	*Schizosaccharomyce spombe*	NP_592974; GI:19113886

Supporting information

Ppk15p	*Schizosaccharomyces pombe*	NP_593830; GI:19114742
Ppk5p	*Schizosaccharomyces pombe*	NP_593081; GI:63054495
Prp4p	*Schizosaccharomyces pombe*	NP_588261; GI:19075761
Dyrk1 (predicted)	*Dictyostelium discoideum*	XP_642598; GI:66817490
Dyrk2 (predicted)	*Dictyostelium discoideum*	XP_628965; GI:66800079
Prp4B	*Dictyostelium discoideum*	XP_641608; GI:66814997
YakA	*Dictyostelium discoideum*	XP_638920; GI:66810395
HPK-1	*Caenorhabditis elegans*	NP_741762; GI:25146827
MBK-2	*Caenorhabditis elegans*	NP_502492; GI:71988995
MBK-1	*Caenorhabditis elegans*	NP_510460; GI:25152628
PRPF4	*Caenorhabditise legans*	NP_492008; GI:17506739
dDyrk2 (Smi35A)	*Drosophila melanogaster*	NP_523564; GI:17737415
dDyrk3 (CG40478)	*Drosophila melanogaster*	NP_001033810; GI:85724756
dHipk (CG17090)	*Drosophila melanogaster*	NP_728531; GI:24654780
Minibrain (dDyrk1)	*Drosophila melanogaster*	NP_728104; GI:24642876
dPrp4 (CG7028)	*Drosophila melanogaster*	NP_612010; GI:19922978
PRP4K	*Homo sapiens*	NP_003904; GI:89276756
HIPK1	*Homo sapiens*	NP_938009; GI:38201640
HIPK2	*Homo sapiens*	NP_073577; GI:164420685
HIPK3	*Homo sapiens*	NP_005725; GI:114796624
HIPK4	*Homo sapiens*	NP_653286; GI:31542768
DYRK1A	*Homo sapiens*	NP_001387; GI:18765758
DYRK1B (Mirk)	*Homo sapiens*	NP_004705; GI:4758222
DYRK2	*Homo sapiens*	NP_006473; GI:153281169
DYRK3 (REDK)	*Homo sapiens*	NP_003573; GI:51702240
DYRK4	*Homo sapiens*	NP_003836; GI:28827774
AtYak1	*Arabidopsis thaliana*	NP_198447; GI:42568145
LinJ.14.0890	*Leishmania infantum*	XP_001464268.1; GI: 146081498
LinJ.14.1140	*Leishmania infantum*	XP_001464290.1; GI: 146081591
LinJ.15.0180 (*Lin*DYRK1)	*Leishmania infantum*	XP_001464356.1; GI: 146081806
LinJ.19.0360	*Leishmania infantum*	XP_001464999.1; GI: 146084408
LinJ.21.2010	*Leishmania infantum*	XP_001465461.2; GI: 339898159
LinJ.33.1930	*Leishmania infantum*	XP_001468297.1; GI: 146098030
LinJ.35.1850	*Leishmania infantum*	XP_001469005.1; GI: 146101011
LinJ.36.4460	*Leishmania infantum*	XP_001470018.2; GI: 339899360

Table shows Fasta (NP) or Uniprot (XP) accession numbers of proteins whose sequences were used for the phylogenetic analysis

S4 Table: List of primers used in PCR reactions.

Ref.	Primer name	Primer sequence	Added restriction sites	Use
p1	pXNG-*Lin*DYRK1 for	5'CTCTAGATCTGGAGCATGGCTGACTCTTCGAAGGTG3'	BglII	*Lin*DYRK1 internal primers and amplification for cloning into [pXNG4]. Forward primer also used with p21 to amplify insert for generating construct [*Lin*DYRK1-carboxyterminal]
p2	pXNG-*Lin*DYRK1_rev	5'CTCTAGATCTCTATTCGGCTGGAGGAAGAGCA3'	BglII	

Supporting information

p3	*Lin*DYRK1 5'UTR_for	5'GTTTAAACCCACTTCCCTCCCTCTGAAC3'	PmeI	5'UTR amplification of for cloning into [pGEM-T]
p4	*Lin*DYRK1 5' 5'UTR_rev	5'ACTAGTTGCTGATCTCCCCCCTTCGC3'	SpeI	
p5	*Lin*DYRK 3'UTR_for	5'GGATCCAGATGGGAGGCAGGCGGCGACTA3'	BamHI	3'UTR amplification for cloning into [pGEM-T easy].
p6	pXNG-*Lin*DYRK1 3'UTR_for	5'GTTTAAACCCTTGAAGGAGAGGCTCCAC3'	PmeI	
p7	hph_for	5'TCATCCGGGTCCGAGCACTAGTGATGAA3'	SpeI intern	Amplification of *hph* gene from [pX63-Hyg] for construction of targeting cassette
p8	hph_rev	5'GACAGGATCCTCTATTCCTTTGCCCTCGGA3'	BamHI	
p9	PAC_for	5'AAGGACTAGTCCTTCCATGACCGAGTACAAG3'	SpeI	Amplification of *hph* gene from [pXG-PAC] for construction of targeting cassette
p10	PAC_rev	5'GTTTGGATCCTAGGCACCGGGCTTGCGGGT3'	BamHI	
p11	PAC_integration_rev	5'CGTGGGCTTGTACTCGGTCATG3'	*	Validation of PAC cassette integration
p12	HYG_integration_rev	5'CATCAGGTCGGAGACGCTGTC3'	*	Validation of HYG cassette integration
p13	internal_DYRK_rev	5'CTCCACCTCATACGGCGCATG3'	*	Cassette integration/ genomic *Lin*DYRK1 copy
p14	Genomic DYRK	5'GTGTGTGGGTTGTTCGTCGAGG3'	*	Presence of genomic *Lin*DYRK1 copy
p15	Meta1_for	5'ATGGAGATGAAAAAACTTGCTTGG3'	*	Amplification of Meta-1 transcript
p16	Meta1_rev	5'TTGATGATGTGTGTTTTAGACTGC3'	*	
p17	HASPB_for	5'ATGGGAACTTCTTGTACAAAG3'	*	Amplification of HASPB transcript
p18	HASPB_rev	5'TCCGTGATTGGCCTCAGT3'	*	
p19	Prohibitin_for	5'CTTCTGCTCATTCTCCATCAG3'	*	Amplification of Prohibitin transcript
p20	Prohibitin_rev	5'CTTAGCGTGACAGCTGC3'	*	
p21	RDYRK1CtermGFP	5'CACAGGATCCTTCGGCTGGAGGAAGAGCA3'	BamHI	Reverse primer used to amplify *Lin*DYRK1 insert with primer p1 for generating construct [*Lin*DYRK1-carboxyterminal]
p22	FGFPN3	5'GTGGGAGGTCTATATAAGCAGAGC3'	* (BamHI site internal inside the amplified product)	Amplification of eGFP from [pEGFP(N3)] for cloning into [*Lin*DYRK1-carboxyterminal], to generate construct [pXG-PAC-*Lin*DYRK1-GFP]
p23	RGFPN3	5'CTCTCAGATCTTTACTTGTACAGCTCGTCCATG3'	BglII	

Table shows the names of the primers and describes the purpose of their use during the experimental procedures